

Surface processes and phase transitions from ab initio atomistic thermodynamics and statistical mechanics

Catherine Stampfl^{a,b,*}

^a*School of Physics, The University of Sydney, Sydney 2006, Australia*

^b*Fritz-Haber-Institut der Max-Planck-Gesellschaft, Faradayweg 4-6, D-14195 Berlin, Germany*

Abstract

Knowledge of the surface composition and atomic geometry is a prerequisite for understanding the physical and chemical properties of modern materials such as those used in, for example, heterogeneous catalysis, corrosion resistance, sensors, and fuel cells. To understand the function of surfaces under realistic conditions, it is crucial to take into account the influence of environmental gas at finite (possibly high) temperatures and pressures. Recent experimental and theoretical studies have shown that when transition metal surfaces are exposed to high oxygen pressures, thin oxide-like structures can form which may have little similarity to the bulk oxides, and thus possess unique chemical and physical properties. Given that technological oxidation catalysis typically involves oxygen-rich conditions, such structures may be present, and in fact be the active material for the reaction, as opposed to the traditionally believed pure metal. Using the approach of ab initio atomistic thermodynamics, free energy phase-diagrams for oxygen/transition metal systems in (T, p) -space ranging from ultra-high vacuum to technically relevant pressures, p , and temperatures, T , are discussed. In addition, results of ab initio statistical mechanical schemes, namely, the Lattice-gas Hamiltonian plus Monte Carlo (MC) simulations, are presented for oxygen/transition metal and alkali-atom/metal systems, where for the latter, the recently introduced “Wang–Landau” algorithm is employed, which affords an accurate estimation of the density of (configurational) states, therefore allowing a direct determination of all major thermodynamic functions.

© 2005 Published by Elsevier B.V.

Keywords: Surface; Phase transition; Atomistic thermodynamics

1. Introduction

One of the main goals of theoretical heterogeneous catalysis, and materials and surface science in general, is to achieve an accurate atomistic description of solids and their surfaces that can predict phenomena and properties occurring on macroscopic length and long time scales. Such methods should quantitatively describe measurable properties without relying on experimental parameters, which implies that they have to start ab initio, i.e., from the self-consistent evaluation of the electronic structure [1,2]. Clearly, knowledge of the surface structure and composition are crucial ingredients for such a description, and consequently for understanding the associated physical and

chemical properties. This is particularly relevant for the long held desire of being able to tailor (and possibly design) functional surfaces for use in a wide range of technological applications such as, heterogeneous catalysis, corrosion resistance, semiconductor and magnetic devices, and fuel cells, to name a few.

The present paper will discuss, through various examples, state-of-the-art first-principles-based theoretical methodology and concepts which are valuable for obtaining a greater understanding and prediction of surface processes and phase transitions at the atomic level, which are of fundamental interest and importance to functional surfaces in general. The paper, largely a review of recent work, is organized as follows: In Section 2, using density-functional theory (DFT), investigations into trends of the initial stage of oxidation at a series of late 4d transition metal (TM) surfaces are described, namely, Ru(0 0 0 1), Rh(1 1 1), Pd(1 1 1),

* Tel.: +49 3084134853; fax: +49 3084134701.

E-mail address: stampflc@fhi-berlin.mpg.de.

and Ag(1 1 1). In Sections 3 and 4, respectively, the O/Ag and O/Ru systems are discussed in detail, where the approach of “ab initio atomistic thermodynamics” is employed. This method allows a comparison of the relative stability of surface structures under varying gas-pressure and -temperature conditions. In Sections 4.1 and 4.2, it is shown how the construction of a Lattice-gas Hamiltonian (LGH), together with both analytic rate equations and Monte Carlo (MC) simulations, can accurately predict new stable phases, as well as the (temperature dependent) heat of adsorption and temperature-programmed thermal desorption (TPD) spectra. In Section 5 the LGH + MC approach is used to study order–disorder phase transitions of Na on Al(0 0 1), where instead of the usual Metropolis MC scheme [3,4], the approach of Wang and Landau is employed [5] in which the (configurational) density of states, CDOS, are explicitly obtained. From the CDOS, the all the major thermodynamic functions can be determined. Finally, in Section 6 the conclusion is given.

All the calculations discussed in the present paper were performed using DFT [6–9] with the generalized-gradient approximation (GGA) for the exchange-correlation functional [10,11]. Either the all-electron full-potential linearized augmented plane-wave (FP-LAPW) [12] method or the pseudopotential plane-wave method [13] was used.

2. On-set of oxidation at transition metal surfaces

The importance of transition metals (TMs) for oxidation catalysis [14–16] has motivated large numbers of studies on oxygen–metal interactions [17,18] at low index surfaces in order to gain a better understanding of the underlying mechanisms [19]. Experimentally, investigations carried out under ultra-high vacuum (UHV) conditions represent the overwhelming majority performed over the last few decades. Here the systems can be well controlled and quantitatively characterized on the microscopic level by a vast array of experimental surface science techniques [20]. On the theoretical side, ab initio investigations of surfaces have typically been limited to zero pressure and zero temperature. Often the results achieved, however, for these situations cannot be extrapolated directly to the technologically relevant situation of finite-temperature and high-pressure. In particular, a possible oxidation of the surface in a reactive environment has often been perceived as leading to an inactive surface oxide layer, poisoning the catalytic reaction. That oxide patches on a surface may instead be the active centers has only recently been indicated in experiments of CO oxidation over Ru(0 0 0 1) and Pt(1 1 0) [21–24]. Accordingly, modern surface science, theoretical and experimental, has realized that bridging this so-called pressure- (and materials-) gap is inevitable [1,2]. As a consequence, there have been many recent interesting findings, including for example that oxidation of transition metal surfaces can lead to the formation of two-dimensional

surface oxides which may or may not bear a resemblance to the corresponding bulk oxides, e.g., the O/Ag(1 1 1) [25–28], O/Pd(1 1 1) [29], and O/Pd(1 0 0) [30,31] systems, and which may not necessarily be thermodynamically stable, e.g. O/Rh(1 1 1) [32], and O/Pt(1 1 0) [33]. In different but related systems, other interesting phenomena have also been reported. For example, the identification of thin metastable surface vanadium oxides on Pd(1 1 1); [34] transition into the stable oxide configuration only occurring beyond a critical thickness. Also, encapsulation of platinum clusters on TiO₂(1 1 0) by a reduced titanium oxide layer has been observed and atomically characterized [35]. These studies highlight the complex nature of surface atomic structures that can form for oxygen/TM systems, and how they depend sensitively upon the “environment”, e.g., the pressure and temperature. Furthermore, the two (or less for the case of clusters) dimensional nature of these films indicate that they may possess unique properties and functionalities that are distinct to the related bulk phases. Indeed, ultrathin films of metal oxides are known to be important materials for solid-state electronic devices, sensors, and for a range of catalytic processes [36–39].

In the present section, we discuss studies addressing initial oxide formation at the basal plane of four 4d TMs, namely, Ru(0 0 0 1), Rh(1 1 1), Pd(1 1 1), and Ag(1 1 1) [40]. On all these surfaces, the O atoms prefer to occupy the three-fold hollow site that corresponds to the stacking type of the substrate, i.e., the hexagonal-close-packed (hcp) hollow sites for Ru and face-centered-cubic (fcc) hollow sites for Rh, Pd, and Ag. These highly coordinated sites are shown in Fig. 1. The adsorption energy (per atom) of atomic oxygen on a surface is calculated as:

$$E_{\text{ad}}(\theta) = -\frac{1}{N_{\text{O}}} [E_{\text{O/Surf}} - E_{\text{Surf}} - N_{\text{O}}E_{\text{O}}], \quad (1)$$

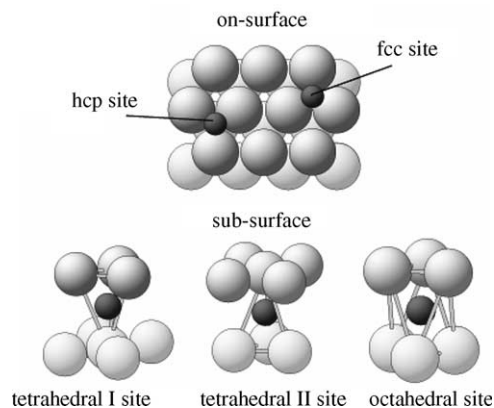


Fig. 1. Highly coordinated adsorbate sites at an fcc(1 1 1) or hcp(0 0 0 1) surface. Upper: top view of the surface where the two three-fold coordinated hollow sites are indicated. Lower: local atomic geometries of the three high-symmetry interstitial sites between the first and second substrate layers. Metal and oxygen atoms are depicted as large and small spheres, respectively.

where N_O is the number of O atoms in the unit-cell at the considered coverage θ (measured in monolayers (ML), which is the ratio of adatoms to the number of atoms in the first metal layer). $E_{O/Surf}$, E_{Surf} , and E_O are the total energies of the adsorbate system, the corresponding clean surface, and the free oxygen atom, respectively. A positive adsorption energy reflects that the adsorption is exothermic. For structures involving “substitutional adsorption” (O atoms occupying metal atom sites), it is assumed that the displaced metal atom binds at a kink site at a step where it gains the cohesive energy [41]. The associated cost of creating the vacancy, i.e., the so-called “vacancy formation energy” must then be taken into account (see Ref. [41]).

The adsorption energies as a function of oxygen coverage are shown in Fig. 2 for the O/Ru(0 0 0 1) and O/Ag(1 1 1) systems. It can be seen that with increasing oxygen coverage, the adsorption energy steadily decreases. This is due to effective repulsive lateral interactions between the adsorbed O atoms: the oxygen atoms are partially negatively charged and when the adlayer becomes more dense this repulsion increases, contributing to the observed decrease in adsorption energy. Also, “through surface” or “substrate-mediated” interactions could be involved as well. Considering the adsorption energy with respect to the experimental (theoretical) binding energy of the oxygen molecule, it can be seen that a full monolayer of O on Ru(0 0 0 1) is predicted to be stable, while on the Ag(1 1 1) substrate, coverages of only about 0.4 ML (0.66 ML) are predicted to be stable. The binding energy of the O_2 molecule as calculated with state-of-the-art GGA functionals is too large by about 0.5 eV per O atom [10,42,43]. Since the binding of adparticles on surfaces as obtained with DFT-GGA are also typically overestimated, but by a lesser degree, some error cancellation will occur when evaluating the adsorption energy with respect to

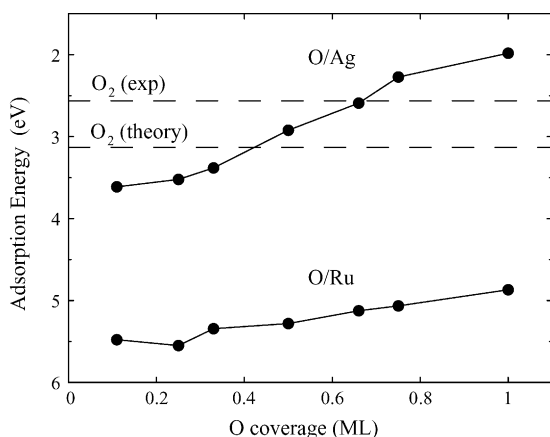


Fig. 2. Adsorption energies, $E_{ad}(\theta)$ (cf. Eq. (1)), of atomic oxygen chemisorption on the surface in the most stable hollow sites of Ru(0 0 0 1) (hcp site) and Ag(1 1 1) (fcc site) with respect to the free O atom. The lines connecting the points are to guide the eye. The theoretical and experimental binding energy of gaseous O_2 (per atom) are indicated by the dashed lines (after Refs. [44,45]).

(1/2) O_2 . Nevertheless, this problem indicates that caution should be exercised when considering the stability (and exothermicity) of oxygen adsorption or oxide formation. For many problems, and the ones discussed in the present paper, adsorption energy ‘differences’, i.e., the relative stability of various structures, are the important quantities. The adsorption energies of O on Rh(1 1 1) and Pd(1 1 1) follow the same trend of decreasing in value with increasing coverages, and lie in between the values of the O/Ru(0 0 0 1) and O/Ag(1 1 1) “extremes”, where O on Rh(1 1 1) has the stronger binding as compared to O on Pd(1 1 1) [40]. Thus, the expected trend of a weaker adsorbate bond on going from left (middle) to right in the periodic table is observed. It is interesting to note that the curves are not completely smoothly varying functions of the coverage, for example, the clear dip for O/Ru(0 0 0 1) at 0.25 ML corresponds to formation of the stable (2×2) phase. These variations reflect the different coordinations and symmetries involved in the various structures.

The above-mentioned trend of a weaker O–metal bond on going from the middle to the right in the periodic table can be understood on the basis of the Anderson–Grimley–Newns model of chemisorption [46–48]. Here, the interaction of the O-2p level with the narrow 4d band of the TM surface gives rise to bonding states at the lower edge of the d band and anti-bonding states at the upper edge of the d band. On moving from the middle to the right in the periodic table, the Fermi level moves systematically from being well in the d band (for Ru) to being well above above it (for Ag), and thus the anti-bonding oxygen–metal states become progressively more occupied [41,49,50]. As a consequence, the bond strength is weakened.

Due to the strongly repulsive interactions that build-up between adsorbed oxygen atoms for increasing coverage, it is conceivable that energetically more favorable atomic configurations exist; for example, occupation of sub-surface sites, or on-set of oxide formation. In particular, King and co-workers [27] proposed that the critical coverage, θ_c^{thd} , at which the transition from a chemisorbed phase to the appearance of an oxidic film occurs is thermodynamically, not kinetically, determined. That is, below θ_c^{thd} , the differential heat of adsorption, $\partial H_{ad}/\partial\theta$, of the chemisorbed phase is higher than the heat of formation of the oxide, ΔH_f [51], while at θ_c^{thd} , they are equal. Using calculated adsorption energies of O on the discussed 4d TM surfaces, the values of θ_c^{thd} can be determined as the coverage at which the heat of formation of the bulk oxide:

$$\Delta H_f = \left[\frac{\partial H_{ad}}{\partial \theta} \right]_{\theta_c^{thd}} \approx \left[E_{ad} + \theta \left(\frac{\partial E_{ad}}{\partial \theta} \right) \right]_{\theta_c^{thd}}. \quad (2)$$

The resulting values were obtained for the four O/TM systems: $\theta_c^{thd} = 0.89$ ML (Ru), 0.59 ML (Rh), 0.50 ML (Pd), and 0.24 ML (Ag) [40]. That is, oxide formation is predicted to occur at lower coverages for the 4d metals further to the right in the periodic table.

While simple and appealing, this model however does not address the ‘microscopic processes’ underlying the phase transition from the two-dimensional adsorbate layer to the three-dimensional oxide. To gain insight into this aspect, Todorova et al. investigated the incorporation of the first O atom into the sub-surface region of the TM surfaces [40]. At fcc(1 1 1) and hcp(0 0 0 1) surfaces there are three high-symmetry sub-surface sites, namely, the octahedral, tetrahedral-I, and -II sites, as shown in Fig. 1. Hereafter, denoted as ‘‘octa’’, ‘‘tetra-I’’ and ‘‘-II’’. The latter is directly below a first layer metal atom.

From extensive DFT-GGA calculations of all relevant combinations of structures involving either on-surface fcc or hcp sites, and the three sub-surface sites, the critical coverage, θ_c , beyond which it is energetically more favorable for O to occupy sub-surface sites as compared to on-surface sites was determined. The investigation was carried out for a range of total oxygen coverage, θ_{tot} , from 0.25 to 1 ML, and for each θ_{tot} , a range of sub-surface oxygen concentrations (of ‘‘coverages’’), $\theta_{\text{sub-surf}}$, was considered. For example, for $\theta_{\text{tot}} = 0.75$ ML and $\theta_{\text{sub-surf}} = 0.25$ ML, it would mean there is 0.5 ML on the surface and 0.25 ML in sub-surface sites. By selecting the lowest energy configuration for each $(\theta_{\text{tot}}, \theta_{\text{sub-surf}})$ combination (and there could be many such configurations at these coverage combinations), contour plots could be obtained. The results are shown in Fig. 3.

For all the studied O/TM systems, the lowest energy structures (or close to) involve on-surface fcc sites and sub-surface tetra-I sites [40,45,52–55]. Fig. 3 shows that for Ru and Rh, on-surface chemisorption is always the most favorable, that is, O incorporation will start only after completion of a full monolayer, largely in accord with experimental findings [21,56–58]. That is, for every value of total oxygen coverage considered, the lowest energy contour line corresponds to zero fraction ($\theta_{\text{sub-surf}}/\theta_{\text{tot}}$) of sub-surface oxygen. It can be noticed however that the ‘‘valley’’ is shallower for Rh. This may explain the small concentration of sub-surface O that has been reported experimentally [59] for coverage less than 1 ML. For Pd the behavior is rather different to Ru and Rh; in particular, for a total oxygen coverage of between 0.75–0.8 ML it can be seen that the lowest energy in the contour plot occurs for a fraction of sub-surface oxygen of 0.25–0.3 ML. That is, the coverage at which sub-surface O becomes favorable compared to continually occupying the on-surface sites, θ_c , is well below 1 ML. For Ag, θ_c is lower still. In particular, while at 0.25 ML on-surface adsorption is energetically preferred, it can be seen that for total oxygen coverages greater than around 1/3 ML, it becomes favorable for oxygen to start occupying sub-surface sites. That is, only a low coverage of on-surface O is stable before additional O prefers to occupy sub-surface sites. The behavior described above is generally consistent with experiments which find surface oxides at

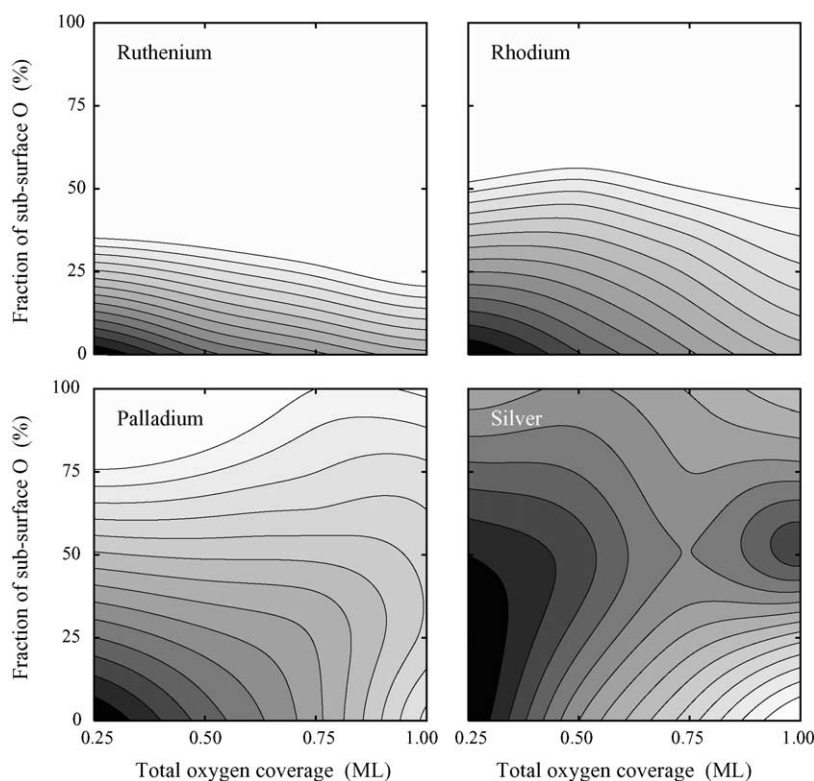


Fig. 3. Average adsorption energy, E_{ad} (cf. Eq. (1)) as a function of the total O coverage, θ_{tot} , of which a certain fraction ($\theta_{\text{sub-surf}}/\theta_{\text{tot}}$) is located below the surface (on-surface in fcc and sub-surface in tetra-I sites). In each case for $\theta = 0.25$ ML, the largest E_{ad} are for pure on-surface chemisorption (black area), with each contour line (lighter grey areas) at 0.1 eV steps for less stable E_{ad} (from Ref. [40]).

Pd(1 1 1) and Ag(1 1 1) with local coverages of about 0.6 ML and 0.4 ML, respectively [27–29].

The values and trend of θ_c , for the initial incorporation of oxygen, are very similar to the O critical coverages beyond which the bulk oxides become thermodynamically stable, θ_c^{thd} discussed earlier. This close relationship suggests that for coverages $\theta_c \approx \theta_c^{\text{thd}}$, not only may O be incorporated into the surface, but oxide formation will begin to take place. In other words, the role of sub-surface O is that of a “metastable precursor”, and the phase transition to bulk oxide formation will proceed nearly instantaneously.

For each of the Ru, Rh, Pd, and Ag TM's, sub-surface O induces a significant expansion of the first interlayer spacing, where the energy cost is highest for the elements to the middle in the periodic table which are “harder” (Ru) and lowest for the “softer” ones to the right (Ag). As described above, the magnitude of the adsorption energy of on-surface chemisorbed O varies significantly between the different TMs, i.e., it is notably stronger on Ru(0 0 0 1) as compared to on Ag(1 1 1) (cf. Fig. 2). The adsorption energy of pure sub-surface oxygen, however, is relatively similar for each metal, and unfavorable [40]. For Ru and Rh the on-surface adsorption energy is sufficiently strong, and even if the energy cost for distorting the substrate was “removed” for the case of sub-surface adsorption, on-surface adsorption would still be more favorable at all coverages. Thus, the preference to adsorb on the surface is an “electronic effect”. This is also true for Pd and Ag, but only for low coverage; due to the respectively lower on-surface adsorption energies of O on these elements, the growing unfavorable lateral interactions between chemisorbed O atoms for increasing coverage, eventually renders on-surface O unfavorable for additional O adsorption and sub-surface incorporation of oxygen becomes energetically favorable. This results in the on-set of sub-surface occupation beginning at progressively lower oxygen coverages for the late 4d TMs in the sequence from Ru to Ag.

In what follows, in order to determine additional similarities, differences, and trends with regard to further oxygen incorporation and oxidation of the TMs, detailed investigations are discussed for the “extremes” of O/Ag(1 1 1) and O/Ru(0 0 0 1) in Sections 3 and 4 below.

3. Surface oxide formation at Ag(1 1 1)

Sabatier in the early 1900s, put forward a concept that a good catalyst should readily dissociate adparticles but not bind the fragments too strongly [60,61]. This translates to the expectation that the reaction intermediates should have an “intermediate” or “moderate” adsorption energy. In this way, the reactants will be bound strongly enough to be stable under the pressure and temperature conditions of catalysis, but not so strongly that reaction with neighboring adparticles will be inhibited. Despite this view, somewhat puzzlingly,

silver, as a noble metal, which binds adparticles only relatively weakly on the surface, as seen in Section 2, is a very important heterogeneous catalyst for various oxidation reactions. For example, the partial oxidation of methanol to formaldehyde, as carried out at atmospheric pressure and temperatures (T) of 800–900 K [62,63], as well as the selective oxidation of ethylene to epoxide, also conducted at atmospheric pressure and at $T = 500$ –600 K [64].

Although the subject of numerous investigations, the active oxygen species involved in these reactions has still not been conclusively identified. For the epoxidation of ethylene, a number of candidates have, however, been proposed; for example, a molecular ozone-like species adsorbed at under-coordinated Ag sites [65], and “bulk-dissolved” oxygen, as well as a “strongly bound, surface-embedded species” [62]. In the previous section, it was shown that on-set of oxidation of Ag(1 1 1) may be expected for relatively low oxygen coverages (~ 0.25 ML). Nevertheless, the presence of disilver oxide (Ag_2O) under reaction conditions was ruled out on the basis that it is thermodynamically unstable under catalytic conditions [63].

To help shed light on the nature of the active species, systematic DFT-GGA calculations by Li et al. [25,26] were performed for all conceivably relevant oxygen species.

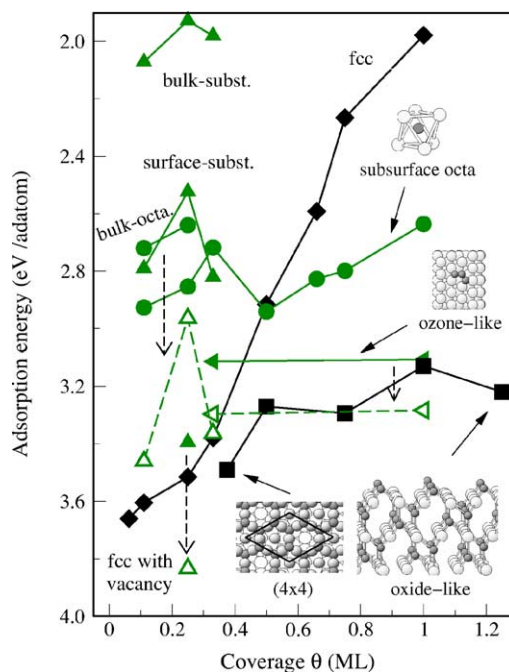


Fig. 4. Selected results of average adsorption energies (cf. Eq. (1)), (with respect to atomic O) vs. coverage for various structures: pure on-surface oxygen in fcc-hollow sites (diamonds), surface- and bulk-substitutional adsorption (triangles), pure sub-surface oxygen in octa sites under the first (“sub-surface-octa.”) and second (“bulk-octa.”) Ag layers (circles), an O_3 -like molecule adsorbed at a surface Ag vacancy (left-pointing triangles), and oxide-like structures (squares). The dashed, downward pointing arrows (and open symbols) indicate the values if the vacancy formation energy for substitutional structures is not considered. In the sketches of atomic structures, oxygen atoms are depicted as small dark spheres and Ag atoms as the larger light spheres (after Ref. [25]).

Experiments indicate that the (1 1 1) surface plays an important role in real silver catalysis in that at high temperature, facets with this orientation result [62,66], thus this surface was chosen for the theoretical investigations. The resulting adsorption energies are summarized in Fig. 4, where for each “type” of site, only the lowest energy one is shown (e.g., on-surface, sub-surface etc). For purely sub-surface O under the first Ag layer, the octa site is most favorable. Adsorption deeper in the bulk in octa or substitutional sites is unfavorable, as seen from the points labeled “bulk-octa” and “bulk-subst.” This result indicates that it is unlikely that there will be high concentrations of bulk-dissolved oxygen, and hence these species are not expected to play an important role in the catalytic reactions. Surface substitutional adsorption can also be seen to be unfavorable. Oxygen chemisorption in fcc sites on under-coordinated Ag atoms (next to an Ag vacancy) is notably stronger than on the ideal terraces, as seen by the point labeled “fcc with vacancy”. If the energy cost to create the vacancy however is taken into account, the energy is less favorable than on the (1 1 1) terrace. The molecular ozone-like species adsorbed at an Ag vacancy, is more favorable than purely sub-surface O; and if the vacancy formation energy is not considered (e.g. if there exists “pre-existing” defects at the surface), the binding becomes even more favorable. The most favorable configuration, however, for coverages > 0.25 ML is a surface-oxide like structure.

The atomic structure of the surface-oxide-like configurations consist of 0.25 ML in on-surface hollow sites and 0.5 ML in between the Ag layers. For increasing O concentrations, the structure “grows” by filling deeper lying sites between the Ag layers as depicted in Fig. 5. This behavior was determined by exhaustive searches for the lowest energy combinations of on-surface fcc and hcp sites, and the three sub-surface sites, as depicted in Fig. 1. The most favorable structure at coverage 0.375 ML is a (4×4) thin surface-oxide which was proposed from scanning tunneling microscopy (STM) studies [27,28]. The

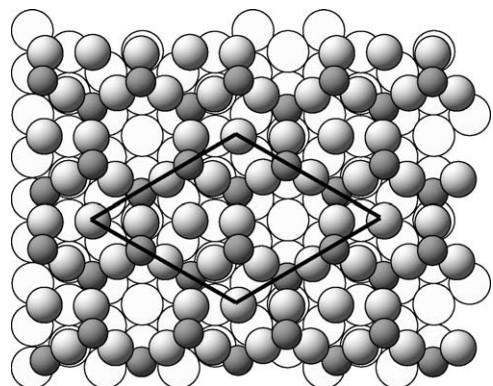


Fig. 5. Sketch of the atomic structure proposed in the STM study of Ref. [28] for the (4×4) phase. The surface unit cell is indicated. The oxygen atoms are represented by small dark circles, the uppermost Ag atoms by grey circles, and the intact plane of Ag(1 1 1) atoms lying below are represented as the open circles (from Ref. [53]).

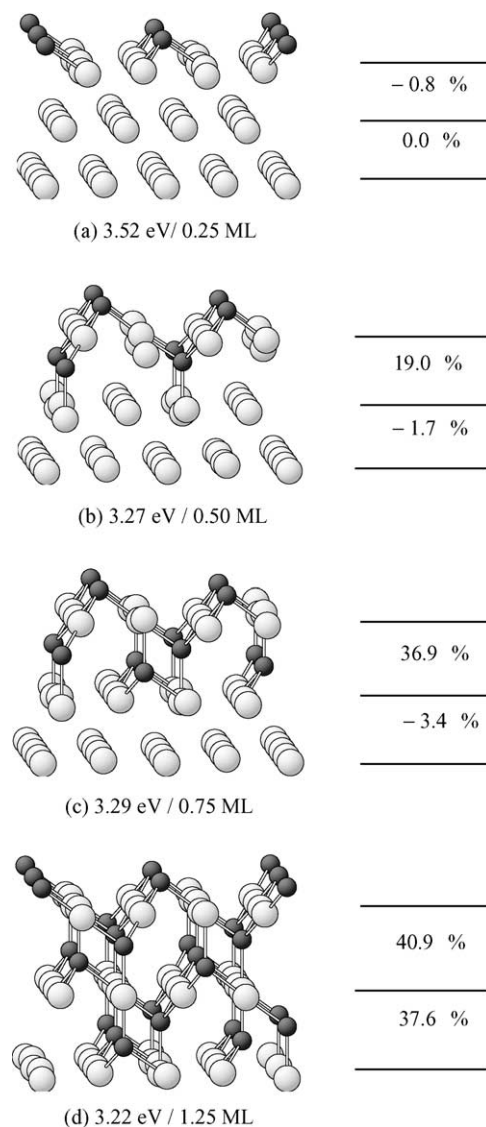


Fig. 6. Atomic geometry of energetically favorable structures for increasing oxygen concentrations: (a) on-surface fcc oxygen, (b) fcc oxygen plus sub-surface oxygen in the tetra-I site, (c) as for (b) but with additional oxygen in the tetra-II site, (d) as for (c) but with additional oxygen under the second Ag layer in the tetra-I and -II sites. The average adsorption energy with respect to the clean Ag(1 1 1) substrate and free oxygen atoms, as well as the corresponding coverage, are given at the bottom of each figure. The relative variation of the first and second interlayer spacings with respect to the bulk value is also given to the right of the figures. Large pale grey and small dark circles represent silver and oxygen atoms, respectively (from Ref. [53]).

atomic structure is shown in Fig. 6. This structure consists of honey-comb-like, silver-oxide “rings” on top of the unreconstructed Ag(1 1 1) substrate, in which the upper O atoms are three-fold coordinated to Ag atoms, and the lower lying O atoms are quasi-tetragonally coordinated to the Ag atoms above and the (1 1 1) substrate below. In the center of each “ring” there is either no additional atoms, or an Ag atom in a hollow site, which is not coordinated to O.

It is interesting to see how the density of states (DOS) differ for purely chemisorbed on-surface oxygen and for the

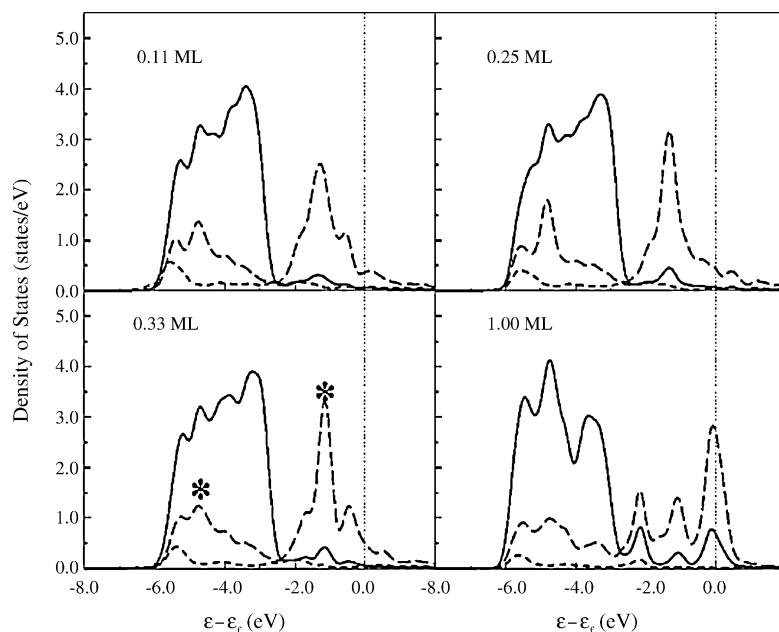


Fig. 7. Projected density of states for the $O/Ag(1\ 1\ 1)$ system with O in the fcc-hollow sites for coverages $\theta = 0.11, 0.25, 0.33,$ and 1.0 ML. The Ag 5s orbital is indicated by a dashed line, the Ag 4d orbital by a solid line, and the O 2p orbital by a long-dashed line. The Fermi energy is indicated by the vertical dotted line. Stars in the $\theta = 0.33$ ML panel indicate the states that are displayed in Fig. 8 (from Ref. [53]).

surface-oxide-like structures. In Fig. 7 the projected DOS [41] for a range of coverages of on-surface O is shown, where the bonding and anti-bonding states are clearly discernable. For the structures with O coverage of 0.11, 0.25, and 0.33 ML where each surface Ag atom is bonded to only one O atom, the DOS look rather similar. For a full coverage of 1.0 ML, however, where each surface Ag atom is bonded instead to three O atoms, the DOS exhibit additional peaks due to the (surface-mediated) hybridization of the states of neighboring O atoms. In Fig. 8 for coverage 0.33 ML, the wave functions for a bonding and anti-bonding state between

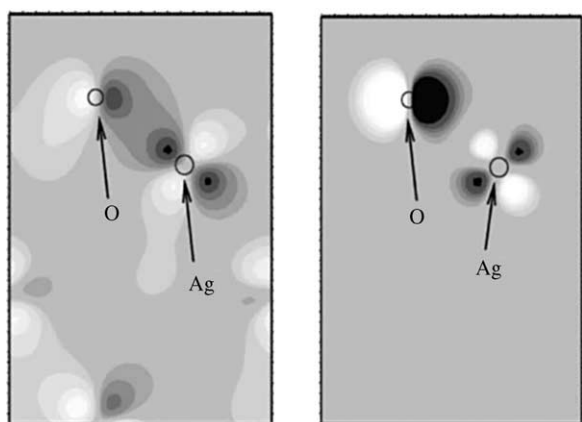


Fig. 8. The wave function of $(\sqrt{3} \times \sqrt{3})R30^\circ-O/Ag(1\ 1\ 1)$ with O in the fcc-hollow site for a bonding state (left) at energy -4.78 eV and an anti-bonding state (right) at energy -1.14 eV, with respect to the Fermi energy at a k -point close to the Γ point (see stars in Fig. 7). The light and dark regions correspond to positive and negative components of the real part of the wave function, respectively. The smaller and large open circles represent the position of the oxygen and silver atoms (from Ref. [53]).

O and Ag atoms are shown. For the bonding state, electron density between the O and Ag atoms can be clearly seen, as can the lack of density, and antisymmetric nature of the wave function at the O and Ag atoms, in the case of the anti-bonding state. For comparison, the projected DOS for the oxide-like structure with a coverage of 1.25 ML (see Fig. 5)

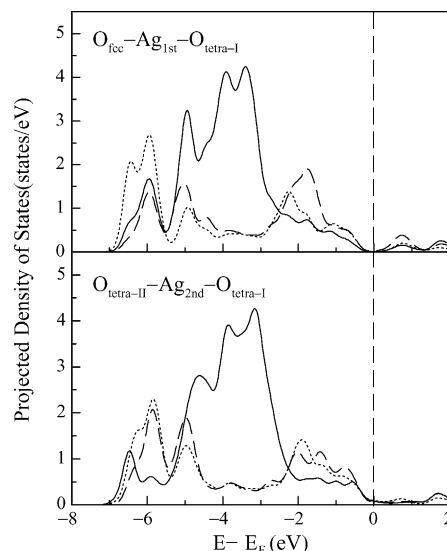


Fig. 9. Total projected density of states for the oxide-like structure ($O_{\text{fcc}}/O_{\text{tetra-I}}+O_{\text{tetra-II}}/O_{\text{tetra-I}}+O_{\text{tetra-II}}\theta=1.25$) as shown in Fig. 5. The upper figure shows the PDOS for O_{fcc} (dashed line), the uppermost Ag atoms bonded to both O atoms (solid line) and $O_{\text{tetra-I}}$ (dotted line) under the first layer. The lower figure shows the PDOS for $O_{\text{tetra-II}}$ (dashed line) under the first metal layer, the shared Ag atom (solid line) and $O_{\text{tetra-I}}$ (dotted line) under the second metal layer. The Fermi energy is indicated by the vertical dashed line (from Ref. [53]).

is shown in Fig. 9. A notable difference to chemisorbed oxygen is that the bonding state now appears well below the Ag 4d band, rather than near the bottom of it, but inside. This behavior is qualitatively the same for the (4×4) structure. It indicates that in experimental studies, this feature could be a “fingerprint” of surface-oxide formation.

To briefly summarize, on the basis of the $p = 0, T = 0$ K, DFT-GGA results shown in Fig. 4, the calculations predict that for low O coverages, oxygen will adsorb on the surface in the fcc site. For increasing coverages greater than around 0.25 ML, formation of the thin (4×4) surface oxide will occur, and then progressively thicker layers with continued oxygen exposure. The calculations do not support either bulk-dissolved or an ozone-like molecule as the active O species for ethylene epoxidation, but point instead to the relevance of thin surface oxides. Below, it will be seen how the stability of the various low energy structures depend on the pressure and temperature conditions.

3.1. Ab initio atomistic thermodynamics: free energy (p, T) phase-diagrams

In ab initio theory, the effect of high temperature and high pressure can be achieved by explicitly taking into account the surrounding gas phase in terms of “ab initio atomistic thermodynamics” [53,67–72]. In this approach the (p, T) phase-diagram can be determined, which describes the surface phases from UHV right up to the conditions of real catalysis [25]. This is also a useful first approach for steady-state catalysis which often takes place close to thermodynamic equilibrium. Here, in the present situation, a surface is in contact with an oxygen atmosphere which is described by the oxygen pressure p and temperature T . This environment acts as a reservoir for O atoms, as it can give (or take) oxygen to (or from) the substrate without changing the temperature or pressure. The surface free energy is calculated as:

$$\Delta G(\mu_{\text{O}}) = -\frac{1}{A}(G_{\text{O/Surf}} - G_{\text{Surf}} - N_{\text{O}}\mu_{\text{O}} - N_{\text{M}}\mu_{\text{M}}). \quad (3)$$

here, A is the area of the surface unit-cell, and $G_{\text{O/Surf}}$ and G_{Surf} the Gibbs free energies of the oxygen/TM system and clean surface, respectively. μ_{O} and μ_{M} the chemical potentials of the oxygen and metal atoms, and N_{O} the number of oxygen atoms contained in the surface structure. N_{M} is the difference in the number of metal atoms between the clean surface and the O/metal surface.

In the difference between the two Gibbs free energies, the vibrational contributions typically exhibit some cancellation. However, when there are additional atomic or molecular species which are not present in the reference system, the situation may be different as there will be no effective cancellation of the contributions of such species between surface and reference systems. For the O/Ag (and O/Ru) systems, it has been nevertheless confirmed that these effects are sufficiently small as not to play an important role

in any conclusions [53,71]. Thus, it is a reasonable approximation to replace the Gibbs free energy difference by the difference of the total energy terms. The T and p dependence is mainly given by μ_{O} , i.e., by the O_2 gas phase atmosphere:

$$\mu_{\text{O}}(T, p) = \frac{1}{2} \left[E_{\text{O}_2^{\text{total}}} + \tilde{\mu}_{\text{O}_2}(T, p^0) + k_{\text{B}}T \ln \left(\frac{p_{\text{O}_2}}{p^0} \right) \right] \quad (4)$$

where p^0 denotes atmospheric pressure and $\tilde{\mu}_{\text{O}_2}(T, p^0)$ includes contributions from rotations and vibrations of the molecule, as well as the ideal-gas entropy at 1 atm. It can be calculated or taken from experimental values listed in thermodynamic tables [73]. The metal chemical potential, μ_{M} is taken to be the metal bulk, with which the surface is assumed to be in equilibrium (i.e. the total energy of an Ag atom in fcc bulk).

On plotting the free energy as a function of oxygen chemical potential for the low energy structures (see Fig. 10), it is apparent that the more oxygen is accommodated in the surface structure, the steeper the slope of the line. In the limiting case of the bulk oxide, with infinite number of O atoms, the line will become vertical at a value of the oxygen chemical potential that equals the bulk oxide heat of formation per O atom. The range of the chemical potential between the vertical dashed lines

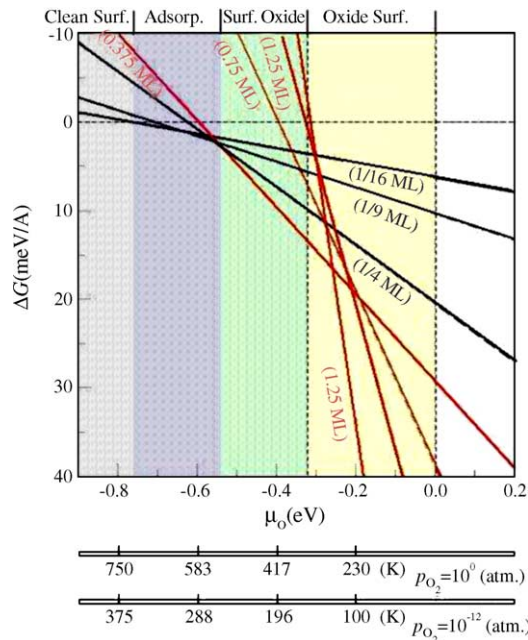


Fig. 10. Surface free energies for O on Ag(1 1 1) for the various low energy structures as a function of the O chemical potential which is defined with respect to $E_{\text{O}_2^{\text{total}}}$. On-surface chemisorbed oxygen with coverages 1/16, 1/9, and 1/4 ML (labeled by these coverages), the (4×4) structure (accordingly labeled “0.375 ML”), commensurate oxide-like structures with coverages 0.75 ML, 1.25 ML, and 2.25 ML (as labeled by the coverages). The corresponding temperatures are given for two selected pressures (cf. Eq. (4)), one corresponding to UHV conditions and the other to the atmospheric conditions of catalysis. The various “types” of surfaces are indicated by the shaded regions, and labeled at the top of the plot (from Ref. [25]).

corresponds to the range in which bulk disilver oxide is stable. The oxygen chemical potential can be correlated with the temperature for a given pressure. This has been done in Fig. 10 for two pressures; one characteristic of UHV, 10^{-12} atm., and the other characteristic of catalysis, 1 atm. Considering the temperatures, it can be quickly noted that bulk disilver oxide, and the thicker oxide-like structures, have a very low thermal stability, and so they can be safely ruled out as playing an important role in the catalytic reactions. For values of μ_{O} further to the left, the (4×4) phase is the most stable for a considerable range of μ_{O} ; in particular, for atmospheric pressure it coincides with temperatures under which epoxidation of ethylene occurs, suggesting it may play an important role in the reaction. For higher temperatures, on-surface adsorbed oxygen is the only stable species. Similar findings have been reported in Ref. [74]. Although not shown in Fig. 10, O atoms adsorbed at under-coordinated surface Ag atoms, such as next to a vacancy or step edge, are stable to considerably higher temperatures (in excess of 860 K), and could possibly be relevant for certain catalytic reactions (e.g., partial oxidation of methanol).

By considering only the lowest energy structures, as a function of pressure and temperature, the phase-diagram shown in Fig. 11 results. It shows that regardless of the pressure, the ordering of the phases is the same. That is, the same phase should be observable at different pressures if the temperature is adjusted accordingly—providing that formation of the structures is not prevented due to kinetic hindering. The result in Figs. 10 and 11 suggest that the thin (4×4) surface oxide could contain the main species actuating ethylene epoxidation since its stability regime coincides with the typical technical conditions. We note, however, that very recently subsequent experimental and theoretical studies indicate that the precise geometry of the (4×4) phase may be somewhat different; to date, however, there is no consensus on this [75]. Identification of a more stable

(4×4) phase would mean that the phase boundary between this structure and the chemisorbed on-surface structures (see Fig. 11) would move to slightly higher temperatures.

In the next section results of similar detailed investigations into the initial oxidation of the Ru(0 0 0 1) surface are discussed.

4. Oxidation of Ru(0 0 0 1)

The motivation for investigating oxygen adsorption and oxide formation at the Ru(0 0 0 1) surface, aside from the wish to better understand the fundamental processes of the oxidation of metal surfaces (or corrosion) in general (an important problem in itself), originated from the following apparent inconsistencies: supported Ru catalysts [76], as well as Ru(0 0 0 1) single crystals [77] have a high reactivity for CO oxidation, under high-pressure and -temperature conditions. However, under UHV conditions [78] the turnover frequency is extremely low. This behavior is a clear example of system that exhibits a so-called “pressure gap” [79].

As described in Section 2, oxygen is stable on the Ru(0 0 0 1) surface right up to a full monolayer coverage. It should be mentioned, that based on early experimental surface science studies, it was widely understood that the saturation coverage was only around 0.5–0.6 ML [78,80]. DFT-GGA calculations, however, subsequently predicted that 1 ML should be stable and is still significantly exothermic [58,81]. This prediction was confirmed by more recent experiments that employed either NO_2 , which readily dissociates in the presence of preadsorbed O atoms (and by annealing to 600 K, the N atoms are removed as NO molecules, which desorb from the surface), or by using significantly higher O_2 pressures than was usual in the hitherto surface science experiments [58]. In this way the kinetic hindering effects that arise for further O_2 dissociation and adsorption for coverages greater than around 0.5–0.6 ML, when using standard O_2 pressures, could be avoided or overcome. Moreover, the calculations predicted that significantly more than 1 ML could be supported at the Ru(0 0 0 1) surface [44].

For oxygen coverages in excess of 1 ML, DFT-GGA calculations for many atomic configurations involving on-surface O in fcc and hcp sites, and the three sub-surface sites, as displayed in Fig. 1, have been performed [52,79,82]. The average adsorption energies as a function of coverage, for selected structures, are shown in Fig. 12. Firstly, considering the filled circles for $\theta > 1$ ML, involving sub-surface oxygen under an ‘unreconstructed’ Ru(0 0 0 1) layer, it can be seen that occupation of sub-surface sites yields a rapid decrease in the energy, as compared to the 1 ML on-surface structure. However, on increasing the coverage from 0.5 ML of sub-surface O to 1 ML, the energy becomes more favorable indicating an attractive interaction between the O atoms towards formation of a 2 ML structure, which contains 1 ML of oxygen on the surface (fcc sites) and 1 ML in sub-

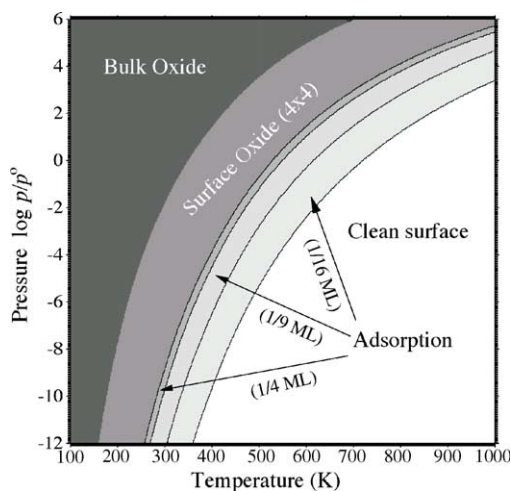


Fig. 11. Calculated (p, T) phase-diagram for the oxygen–Ag(1 1 1) system showing the stable structures (from Ref. [25]).

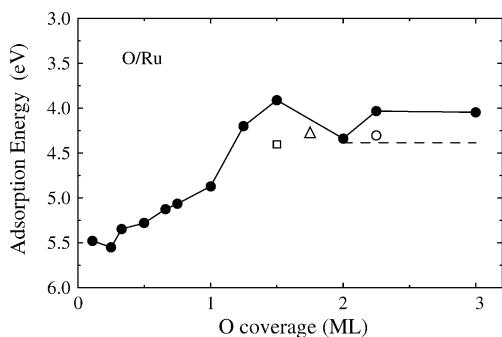


Fig. 12. Average adsorption energy for selected O/Ru(0 0 0 1) structures vs. coverage. For coverages ≤ 1 ML, O atoms occupy on-surface hcp sites. For coverages > 1 ML, the filled circles are structures containing sub-surface oxygen under an *unreconstructed* Ru(0 0 0 1) layer (plus 1 ML on-surface oxygen). The open circle represents a structure as for the 2 ML O–Ru–O trilayer (cf. Fig. 13), but with 0.25 ML O adsorbed on top of a surface Ru atom (cf. Fig. 14). The open square represents the $(\sqrt{3} \times \sqrt{3})R30^\circ$ trilayer-like structure on a (2×2) surface unit cell (see text), and the open triangle as for the latter, but with an O atom adsorbed on top of a surface Ru atom. The horizontal line represents the value of the heat of formation per O atom of bulk RuO₂ (relative to a free O atom) (after Ref. [44]).

surface (tetra-I) sites. The atomic geometry of this so-called “O–Ru–O trilayer” structure is displayed in Fig. 13.

On increasing the coverage from 2 to 2.25 ML, it was found the additional oxygen atoms prefer to bind *on top* of surface Ru atoms, as compared to being incorporated under the first Ru layer in tetra-II sites (compare filled and open circles for coverage 2.25 ML) in Fig. 12. For 3 ML of oxygen, the most favorable structure that has been identified to date is as for the 2 ML trilayer structure, but with 1 ML of sub-surface oxygen occupying tetra-II sites under the first Ru layer. In this geometry the upper O–Ru–O trilayer moves significantly outwards from the surface and is bound only very weakly to the underlying structure (Fig. 14). On the basis of this finding, a mechanism for a phase transition (a so-called “accordian” transformation) to RuO₂(1 1 0) was proposed [82], which is sketched in Fig. 15. Briefly, it

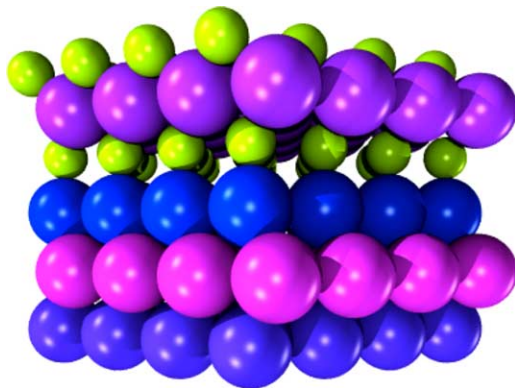


Fig. 13. Atomic geometry of the O–Ru–O trilayer structure which contains 2 ML of oxygen. Large and small spheres represent Ru and O atoms, respectively.

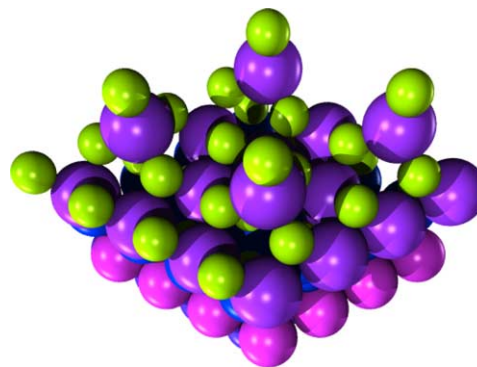


Fig. 14. Atomic geometry of the O–Ru–O trilayer with oxygen adsorbed on top of surface Ru atoms, for 2.25 ML of oxygen. Large and small spheres represent Ru and O atoms, respectively.

was recognized that the trilayer structure is related to RuO₂(1 1 0) by a simple expansion and rotation of O–Ru bonds. In particular, the O–Ru–O components rotate, resulting in alternate bridging O atoms, and in coordinatively unsaturated Ru atoms.

Other possible geometries have also been investigated for the O/Ru(0 0 0 1) system. In particular, for O/Rh(1 1 1), a ‘metastable’ trilayer-type of surface-oxide was identified on the basis of STM and DFT-GGA, which can be described as an (8×8) hexagonal oxide on a (9×9) Rh(1 1 1) surface unit cell [32]. The DFT-GGA calculations in Ref. [32] showed that the stability of the structure was very similar to that when calculated using a smaller (2×2) cell which contained three metal atoms and six O atoms in the uppermost layers, resulting in a RhO₂ stoichiometry that could be described as a $(\sqrt{3} \times \sqrt{3})R30^\circ$ oxide layer on a (2×2) Rh(1 1 1) surface unit cell [32]. DFT-GGA calculations for this latter type of structure, but for the O/Ru system, have been performed and the average adsorption energy is shown as the open square in Fig. 12. Also adsorption of an O atom on one of the three uppermost surface Ru atoms was considered and the most favorable configuration resulted in the average adsorption energy shown as the open triangle in Fig. 12. Interestingly, it can be seen that for the same coverage, these geometries are ‘more favorable’ than those involving an ‘unreconstructed’ Ru(0 0 0 1) surface (filled circles). The heat of formation per O atom of RuO₂ (referred to atomic oxygen, and shown as a horizontal dashed line in Fig. 12), is very similar to the average adsorption energy of the latter described configurations, and to the 2 ML trilayer.

To determine which structures are stable when in contact with an O₂ gas phase, at various pressures and temperatures, again *ab initio* atomistic thermodynamics can be used. The resulting free energy plot is shown in Fig. 16. For $\mu_{\text{O}} < -2.7$ eV the clean surface is most stable, while five different O adsorbate phases with increasing coverages become progressively more stable for more O-rich environments; namely, (2×2) , (2×1) , $(\sqrt{3} \times \sqrt{3})R30^\circ$ -2O, (for a very small range of μ_{O}), (2×2) -3O, and (1×1) .

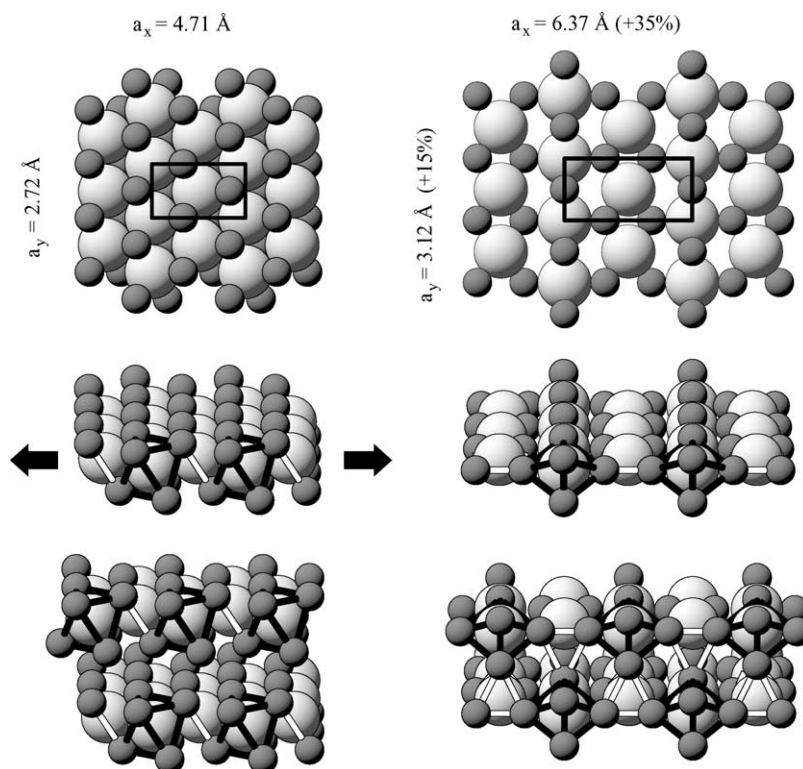


Fig. 15. Atomic geometry of the O–Ru–O trilayer(s) (left) and the rutile $\text{RuO}_2(1\ 1\ 0)$ oxide structure (right). Top panel: top view; middle panel: perspective view. The bulk-like rutile structure can be realized by expansion of the trilayer in direction of the arrows. In this way the length of the O–O bonds (white and black lines) remain essentially unchanged. Bottom panel: two trilayers (left) as compared to the corresponding rutile layers (right). The trilayers hardly bind to each other, while in the rutile layers, bonds form between them (from Ref. [82]).

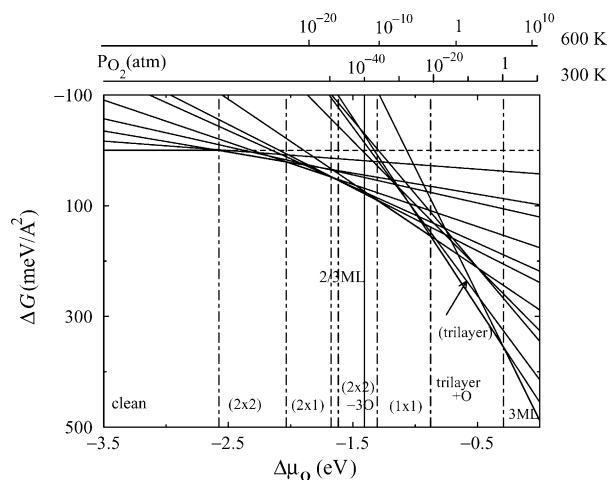


Fig. 16. Calculated free energy for selected low energy O/Ru structures. The chemical potential is given with respect to $1/2E_{\text{O}_2}^{\text{total}}$. The various stable phases are given along the bottom of the plot, where the label “2/3 ML” indicates the $(\sqrt{3} \times \sqrt{3})R30^\circ-2\text{O}$ structure which is only stable for a very narrow region of the oxygen chemical potential. In particular, the stable phases are: $(2 \times 2)\text{-O}$, $(2 \times 1)\text{-O}$, $(\sqrt{3} \times \sqrt{3})R30^\circ-2\text{O}$, $(2 \times 2)\text{-3O}$, and $(1 \times 1)\text{-O}$. The three thin lines represent only metastable structures and correspond to chemisorbed O at 0.33 ML, and the trilayer-like $(\sqrt{3} \times \sqrt{3})R30^\circ$ on a (2×2) unit cell configuration, with and without an O atom adsorbed on top. The vertical continuous line marks the theoretical heat of formation of RuO_2 per O atom.

For $\mu_{\text{O}} > -1.4$ eV, bulk RuO_2 represents the most stable phase. The stability range of this bulk oxide is large, and as can be determined from Eq. (4) (and as indicated by the pressure scale in Fig. 16), it encompasses all realistically attainable pressures for temperatures below about 600 K. All the structures involving sub-surface oxygen, including the reconstructed trilayer-like $(\sqrt{3} \times \sqrt{3})R30^\circ$ oxide in a (2×2) unit cell configuration, are not thermodynamically stable, meaning that they could only act as metastable intermediates that are stabilized by kinetic limitations, before full bulk oxide formation occurs. Interestingly, the O–Ru–O trilayer with 0.25 ML of O adsorbed on top of the surface Ru atoms is more stable than the “plain” 2 ML trilayer structure. It can be seen from Fig. 14 that the on-top O atoms “pull” the Ru atoms far out of the plane, and the structures appears rather like adsorbed RuO_4 molecules. In this respect, Ru_xO_y molecules have been detected (including RuO_4) in experiments investigating the O/Ru system under various (p, T) conditions and the associated structures that form [83]. This suggests that prior to, and in the process of, transformation to the bulk oxide, the surface may become roughened due to the formation of such molecules. This presents an alternative or additional picture to the so-called “accordian transition” for the phase transformation towards full oxidation.

There is a growing consensus that ruthenium dioxide is responsible for the high activity of CO oxidation, due to the identification of its presence on the surface in reactive environments [21,57,84,85]. Interestingly, however, recent experiments have shown that the same order of magnitude for the reaction probability of CO oxidation over Ru surfaces containing RuO₂ domains, is obtained from Ru(0 0 0 1) surfaces loaded with around 3.5 ML in the sub-surface region, *without* the presence of RuO₂ domains [86]. This suggests that intermediate precursor structures are stabilized and also play an active role for CO oxidation.

Considering the O/Pd(1 1 1) system, similarly to the O/Ag(1 1 1) case, a thin, so-called “($\sqrt{6} \times \sqrt{6}$) pseudo-commensurate surface oxide structure” has been identified [29,87], which represents a ‘thermodynamically stable’ phase for a certain range of the oxygen chemical potential. Furthermore, for the O/Pd(1 0 0) system, a thin surface oxide layer with a ($\sqrt{5} \times \sqrt{5}$)R27° periodicity has been identified, which also represents a stable phase [30,31].

With regard to the role that metal oxides may play in heterogeneous oxidation catalysis, it is interesting to consider again the Sabatier principle of the “intermediate” reactant bond strength as an indication of how reactive a particular species may be: For chemisorbed oxygen on Ru(0 0 0 1) the bond strength is very strong, and accordingly the catalytic activity of O/Ru(0 0 0 1) under UHV conditions is very low. With the discovery that RuO₂(1 1 0) films form at the surface in typical reactive environments [21,57,85], the high catalytic performance could be understood, since the binding of oxygen in the oxide is considerably weaker, or of “intermediate” strength. Similarly, but in an opposite manner, oxygen binds to Ag(1 1 1) only very weakly, which on the basis of the Sabatier principle, is difficult to reconcile with the known importance of Ag as an oxidation catalyst. However, the bond strength of oxygen in the $p(4 \times 4)$ surface oxide—that is, the energy to remove the uppermost O atom—is substantially higher and constitutes, rather, an intermediate bond strength [26]. Thus, it appears that the interaction of oxygen with transition metal catalysts can serve to “tune” the O–metal bond strength for optimum reactivity through formation of various oxide-like species.

It is clear that an understanding of the complex atomic configurations that form under varying reaction conditions is only beginning to emerge and calls for on-going quantitative experimental studies, at best carried out in situ, as well as in conjunction with first-principles based investigations.

4.1. Ab initio Lattice-gas Hamiltonian

Having seen the usefulness of the ab initio atomistic thermodynamics approach in the above sections, and noted its main drawback which is that its predictive power is limited to the structures that have been explicitly considered and calculated, the ab initio LGH + MC approach offers greater flexibility in its predictive ability. It is a relatively

newly emerging procedure and represents a “new direction” in the area of ab initio theoretical surface science. In particular, it affords identification of unanticipated geometries and stoichiometries, describes the coexistence of phases and disordered phases, as well as associated order-order and order–disorder phase transitions. It is quite general and flexible, and offers a systematic and efficient procedure for reliably investigating or “screening” configurational space.

In this approach a system is defined by the occupation of the sites in the lattice, and the total energy is written as an expansion of a sum of interactions between these lattice sites. For a system with one species and one site type, the LGH would then, for example, read (generalizations to multi-species and -site systems is straightforward):

$$H = F \sum_i n_i + \sum_{m=1}^{\text{pair}} V_m^{\text{pair}} \sum_{(ij)_m} n_i n_j + \sum_{m=1}^{\text{trio}} V_m^{\text{trio}} \sum_{(ijk)_m} n_i n_j n_k + \dots, \quad (5)$$

where the site occupation numbers $n_l = 0$ or 1 depending upon on whether site l is empty or occupied, and F is the free energy of an isolated species, including static and vibrational contributions. V_m^{pair} are the two-body (or pair) interaction energies between species at m th nearest neighbor sites and V_m^{trio} is the energy due to three-body (or trio) interactions. In principle, higher order interaction terms (quarto, quinto, ...) would follow in this infinite expansion, but in practice, the series is truncated after a finite number of terms. Fig. 17 (left) illustrates some of these interactions. In other fields, this methodology may be called an “Ising-type model” [88] or a “cluster-expansion” [89,90].

Clearly, the Hamiltonian can be evaluated for any lattice occupation, be it dense or sparse, periodic or disordered.

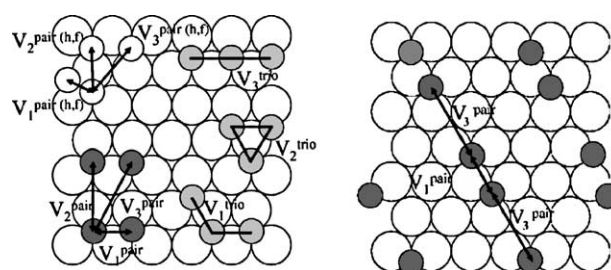


Fig. 17. Left: Some types of lateral interactions for adsorbates that can occupy the two three-fold hollow sites of a hexagonal close-packed surface. V_n^{pair} ($n = 1, 2, 3$) are two-body (or pair) interactions at first, second and third nearest neighbor distances of like hollow sites. V_n^{trio} ($n = 1, 2, 3$) are three three-body (or trio) interactions between three atoms in like nearest neighbor hollow sites, and $V_n^{\text{pair}(h,f)}$ ($n = 1, 2, 3$) represent pair interactions between atoms that occupy unlike hollow sites (i.e. one in fcc and the other in hcp). Right: An adsorbate arrangement from which an expression can be obtained for obtaining interaction parameters. The (3×3) periodic surface unit-cell is indicated by the large darker spheres. The arrows indicate interactions between the adsorbates. Apart from the obvious first nearest-neighbor interactions (short arrows, V_1^{pair}), also third nearest-neighbor two-body interactions (long arrows, V_3^{pair}) exist, due to the periodic images outside of the unit-cell (from Ref. [2]).

Since the approach involves only performing an algebraic sum over a finite number of terms, it is computationally very fast. The most difficult task in constructing the LGH is deciding upon the number and kind (e.g. pair, trio, multi-body) of interaction terms in the expansion to include, and extracting these from DFT calculations. We note that there is no a priori way to know at how many, and what type of, interactions to terminate the expansion. While there are some attempts to automatize this procedure [91] the actual implementation is a delicate task. Some criteria to test the convergence of the Hamiltonian include its ability to predict the energies of a number of DFT-computed configurations that were not employed in the fit, or that it reproduces the correct lowest energy configurations at $T = 0$ K [90]. A limitation is that for more complex systems with multiple sites and several species, the construction of the LGH becomes very complicated.

Traditionally, in applications of the LGH, the interaction parameters have been assumed to be just pairwise additive (i.e., higher order terms beyond pair interactions were neglected) and the interaction energies obtained by simply fitting to experimental data (see, e.g., Refs. [92–94]). This procedure obviously results in “effective parameters” with an unclear microscopic basis, “masking” the effect and possible importance of three-body (trio) and higher order interactions. This means that the thus constructed Hamiltonian is unlikely to be transferable to calculations of other properties of the system. The important role of higher-order, many-atom interactions has recently been pointed out by a number of studies (see e.g. Refs. [79,95–97]).

The appealing aspect of determining the interaction parameters from first-principles calculations is firstly that the treatment is consistent, and there is a “microscopic” meaning to the parameters. To obtain the interaction parameters using typical DFT calculations, which employ a supercell, the interactions between the periodic images are exploited. For this, different configurations in various supercells are computed, and the obtained energies

expressed in terms of the corresponding interatomic interactions. Fig. 17 (right) illustrates this for two atoms adsorbed at neighboring sites in a (3×3) surface unit cell: due to the periodicity, each atom has images in the neighboring cells, and because of this, each atom experiences not only the obvious pair interaction at the first neighbor distance, but also a pair interaction at the third neighbor distance (neglecting higher pairwise or multi-body interactions). The computed DFT adsorption energy for this configuration i , per atom, can then be written as:

$$E_{\text{DFT}}^{(3 \times 3),i} = E + \frac{1}{2}(V_1^{\text{pair}} + V_3^{\text{pair}}), \quad (6)$$

where E is the adsorption energy of an isolated adatom. (The factor $1/2$ arises since the pair interaction is “shared” between two adsorbates.) Doing this for a set of different configurations thus generates a system of linear equations that can be solved for the interaction energies either by direct inversion or by fitting techniques.

One of the first such studies employing the ab initio LGH was of the O/Ru(0 0 0 1) system [79]. In this investigation two kinds of sites (hcp and fcc) were considered and pair interactions up to third neighbor were included, as well as three trio interactions. Using the constructed LGH in combination with rate equations [98], temperature-programmed desorption (TPD) spectra were calculated (see Fig. 18). The rate of desorption was calculated as [99]:

$$R_{\text{des}} = 2S_{\text{dis}}(\theta, T)a_s \frac{k_B T}{h\lambda_m^2} \frac{Z_{vr}}{q_3^2} \frac{\theta^2}{(1-\theta)^2} e^{\frac{-2|V_0|}{k_B T}} e^{\frac{2\mu^{(\text{lat})}}{k_B T}}. \quad (7)$$

here Z_{vr} is the partition function accounting for the internal vibrations and the rotations of O_2 in the gas phase. $\mu^{(\text{lat})}$ is the contribution to the chemical potential of the adsorbate due to the lateral interactions in the Hamiltonian (Eq. (5)), and was calculated using transfer matrix techniques [98,99]. P_m the molecular pressure above the surface, a_s is the area of one unit cell of the substrate surface, $\lambda_m = h/(2\pi mk_B T)^{1/2}$ is the thermal wavelength of a molecule of mass m , and

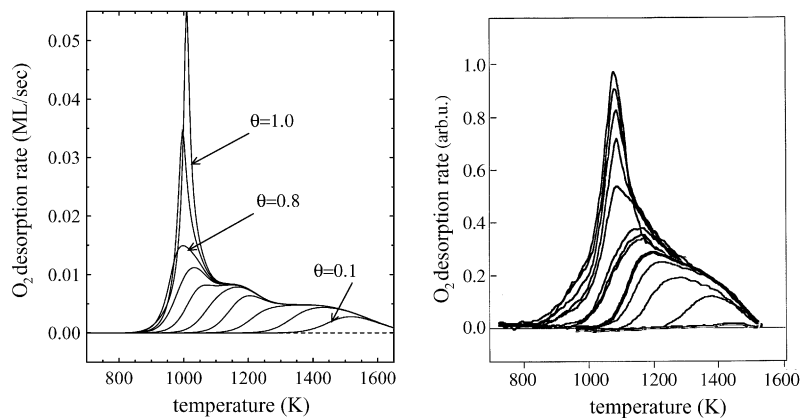


Fig. 18. Temperature-programmed desorption curves: theoretical (left) and experimental (right). Each curve shows the rate of oxygen molecules that desorb from the Ru(0 0 0 1) surface as a function of temperature, when the system is prepared with a given initial oxygen coverage θ ranging from 0.1 to 1 monolayer. The first-principles LGH employed in the calculations is the same as the one underlying the phase-diagram of Fig. 20 (from Ref. [79]).

$S_{\text{dis}}(\theta, T)$ is the dissociative sticking coefficient. Regarding the sticking coefficient, for low coverages up to around 0.5–0.6 ML dissociation is not activated (i.e., there is no energy barrier for dissociation), however for (local) coverages greater than this, it is hindered by an energy barrier [58,80]. Under these circumstances, it would be a significant undertaking to obtain the coverage and temperature dependence of the sticking coefficient ab initio. Therefore an analytic expression which well approximates the measured behavior in the temperature regime of desorption was used, namely $S_{\text{dis}}(\theta) = S_0 \exp[-(\theta/\sigma)^2]$, with $S_0 = 0.27$ and $\sigma = 0.3$ [79].

The theoretical spectra shown in Fig. 18 reproduce all the features of the experimental data. The main deviation is that for low initial coverages (curve with smallest area underneath), oxygen is predicted to desorb at around 100 K higher than experiment, reflecting the overbinding of the O atoms, which is characteristic of DFT-GGA. Furthermore, the isosteric heat of adsorption was determined (Fig. 19), that is, the energy that the O_2 molecule gains by dissociatively adsorbing on the surface. The peaks and dips in the curves reflect the formation of ordered phases. The result clearly predicts the phases with coverages 0.25, 0.5, 0.75 ML. Also, a shoulder is present at 0.66 ML, hinting at the existence of an ordered structure with this coverage. It should be mentioned that at the time of this study, the periodic structure with 0.75 ML had not been experimentally observed, which demonstrates the predictive nature of this first-principles approach. Subsequent experiments by two groups confirmed its existence and quantitatively characterized it [100,101].

The LGH can also be used in conjunction with Monte Carlo simulations. This has been done for the $\text{O}/\text{Ru}(0\ 0\ 0\ 1)$ system and the results are described in the next subsection.

4.2. Equilibrium Monte Carlo simulations

The well-known Metropolis Monte Carlo algorithm [3] aims at obtaining the canonical distribution at a given energy and temperature. It proceeds by generating random configurations. If a new configuration exhibits a lower

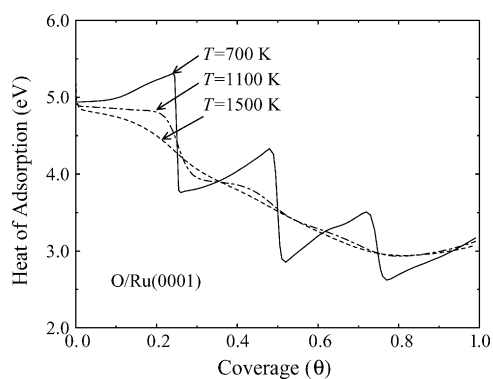


Fig. 19. The heat of adsorption of O_2 on $\text{Ru}(0\ 0\ 0\ 1)$ as a function of coverage for various temperatures. The peaks and dips correspond to ordered phases (from Ref. [79]).

energy than the previous one, it is “accepted”, building-up a sequence of configurations. If the configuration has a higher energy, it still has an appropriately Boltzmann-weighted probability to be accepted into the sequence, otherwise it is “rejected”. The scheme provides a correct sampling of the configuration space, and also fulfills “detailed balance”, that is, the forward probability of accepting a new configuration j from state i is related to the backward probability of accepting configuration i from state j , by the free energy difference of both configurations.

Using the LGH described above, which provides the energies of the various configurations generated, McEwen et al. [102] determined the phase-diagrams shown in Fig. 20. The regions in which the identified phases exist (indicated by capital letters) were determined by an appropriate “order parameter” which identifies lateral periodicities. It can be seen that in the coverage range considered, i.e., from very low coverage up to 0.75 ML, four-ordered structures are

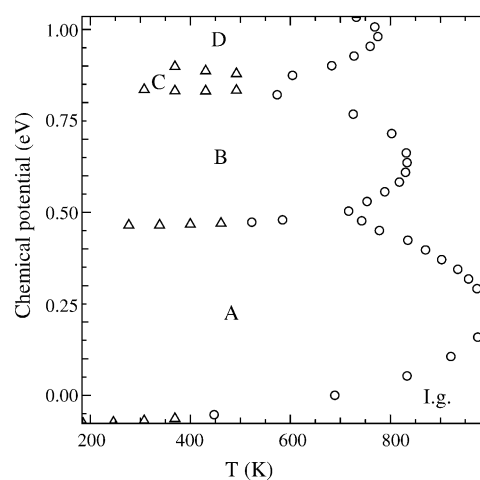
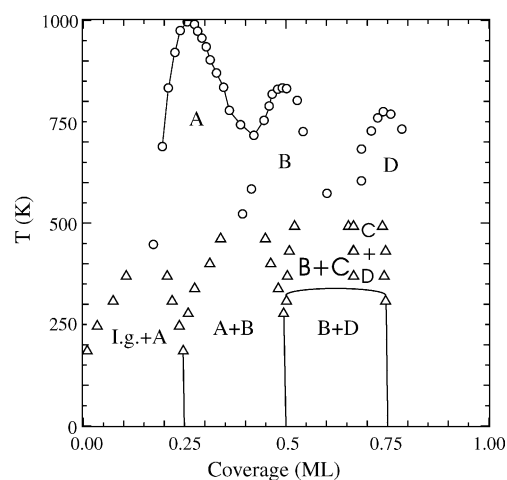


Fig. 20. Phase-diagram for $\text{O}/\text{Ru}(0\ 0\ 0\ 1)$ as obtained using the ab initio LGH approach in combination with MC calculations. Upper: temperature vs. coverage, and lower: oxygen chemical potential vs. temperature. The triangles indicate first-order transitions and the circles second-order transitions. The identified ordered structures are labeled as: $(2 \times 2)\text{-O}$ (A), $(2 \times 1)\text{-O}$ (B), $(\sqrt{3} \times \sqrt{3})R30^\circ$ (C), $(2 \times 2)\text{-3O}$ (D), and disordered lattice-gas (l.g.) (from Ref. [102]).

predicted. Namely, the (2×2) -O, (2×1) -O, $(\sqrt{3} \times \sqrt{3})R30^\circ$ -2O, and (2×2) -3O. Also a disordered lattice-gas was identified, as well as four coexistence regions involving the phases (i) (2×2) -O and (2×1) -O, (ii) (2×1) -O and (2×2) -3O, (iii) (2×1) -O and $(\sqrt{3} \times \sqrt{3})R30^\circ$ -2O, and (iv) $(\sqrt{3} \times \sqrt{3})R30^\circ$ -2O and (2×2) -3O. These phases have all been verified experimentally, with the exception of $(\sqrt{3} \times \sqrt{3})R30^\circ$ -2O which is awaiting confirmation. This latter phase appears only in a very narrow temperature and coverage window so its identification may prove a challenge. The triangles indicate that the transition is of first-order, occurring abruptly, while the circles represent second-order transitions, which occur more gradually.

Clearly the ab initio atomistic thermodynamics and the LGH approaches yield the same results concerning the predicted ordered phases; however, in the former approach this relied upon the thought to actually consider the 2/3, 3/4, and 1 ML structures (which had not hitherto been experimentally identified in the literature), whereas with the LGH, all phases come out “automatically”, without the necessity of such fore-thought.

In what follows, the LGH + MC approach is applied to another system, namely, sodium on Al(0 0 1).

5. Order–disorder phase transitions in Na on Al(0 0 1)

The interest in alkali-metal adsorption systems has been intense, especially since the early 1990s when it was found, first for Na (and K) on Al(1 1 1) and then for Na on Al(1 0 0), that the alkali-metal atoms kick-out surface Al atoms and adsorb in their place, i.e., “substitutionally”. This behavior strongly deviated to the generally accepted picture at the time, which was that alkali-metal atoms adsorb in the highly coordinated on-surface hollow sites, and cause little disturbance to a close-packed metal surface [103–105]. For Na on Al(0 0 1), at a coverage of 0.2 ML, recently a reversible phase transition has been observed in low energy electron diffraction experiments. At low temperature, an ordered $(\sqrt{5} \times \sqrt{5})R27^\circ$ structure forms (see inset of Fig. 22 b), where the Na atoms occupy surface substitutional sites. At temperatures in the range of 220–300 K on the other hand, the Na atoms, still substitutional sites, form a ‘disordered’ arrangement in the surface. Also, below this temperature, reversible order–disorder phase transitions occur as a function of Na coverage (θ_{Na}). In particular, for $\theta_{\text{Na}} < 0.17$ ML a disordered structure occurs, while for increasing coverage to $0.17 \text{ ML} < \theta_{\text{Na}} < 0.23 \text{ ML}$ the ordered $(\sqrt{5} \times \sqrt{5})R27^\circ$ phase forms. For $\theta_{\text{Na}} > 0.23 \text{ ML}$ a disordered phase occurs again, which, with higher coverage gradually transforms into patches of $c(2 \times 2)$ with a local coverage of 0.5 ML, and finally for 0.5 ML the $c(2 \times 2)$ results.

The Na/Al(0 0 1) system has been studied by Borg et al. [106] using the ab initio LGH + MC approach outlined above. In this study, pair interactions up to sixth nearest

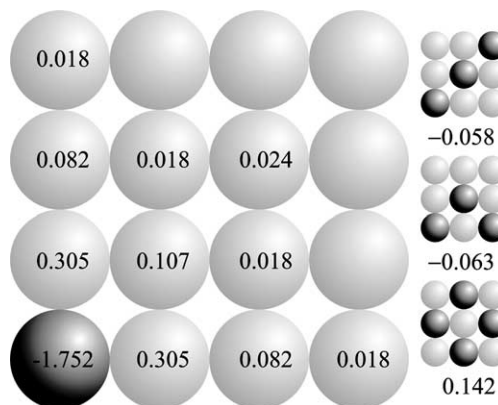


Fig. 21. Sodium interaction energies: pair interactions (V^{pair}) to the left and the two considered trio interactions (V^{trio}) and quarto interaction (V^{quarto}) to the right. The units are eV and a positive value indicates a repulsive interaction. The adsorption energy of an isolated Na atom is given on the dark grey atom (left). For the case of pair interactions, the values of the interactions written on the various “atoms” indicate that between the said atom and the atom located at the darker shaded atom (isolate Na). For example, the second nearest-neighbor pair interaction is 0.107 eV. As may be expected, the values generally decrease with increasing distance between adsorbates (from Ref. [106]).

neighbor, and two trio interactions, and one quarto, were included in the LGH expansion. These are depicted in Fig. 21. They were obtained from $N = 25$ DFT-GGA calculations of various atomic configurations, where the “leave-many-out cross-validation” (LMO-CV) scheme [107,108] was used to obtain the interaction parameters. Briefly, in LMO-CV, $N - d$ DFT-GGA-calculated structures are used in a least-squares fit to obtain the interaction parameters, and the remaining d structures are used to calculate the root-mean-square of the deviations between the LGH-obtained energies, and the DFT-GGA energies (so-called “prediction errors”). This procedure is repeated for many random divisions of the total set, yielding an average prediction error. Furthermore, this procedure is performed for a number of different possible sets of interaction parameters—in this study 24 sets were considered. Then, the parameters yielding the lowest average prediction error are then selected. Carrying out standard MC simulations using these interaction parameters the experimental (temperature-coverage) phase-diagram is well reproduced. Because however, the standard Metropolis scheme is rather inefficient for finding phase transition temperatures, extracting the specific heat, and directly determining the free energy and entropy, we have employed the MC algorithm of Wang and Landau [5]. While most conventional MC algorithms, such as “Metropolis importance sampling”, generate a canonical distribution at a given temperature, the Wang–Landau formalism focusses instead on obtaining an accurate estimate of $g(E)$ (i.e., the number of system configurations with a certain energy E), which is independent of temperature. That is, the so-called (configurational) density of states (CDOS). This is achieved by performing a random walk in “energy space”. From $g(E)$ all major

thermodynamic functions can be directly determined. The canonical distribution at a given temperature is:

$$P(E, T) = g(E)e^{-E/k_B T}, \quad (8)$$

where k_B is the Boltzmann constant; the free energy:

$$F(T) = -k_B T \ln \sum_E g(E)e^{-E/k_B T} = -k_B T \ln(Z), \quad (9)$$

where Z is the partition function; the internal energy:

$$U(T) = \frac{\sum_E E g(E)e^{-E/k_B T}}{Z}, \quad (10)$$

and the entropy:

$$S = \frac{(U - F)}{T}. \quad (11)$$

Fig. 22a shows the calculated CDOS, $g(E)$. The logarithm of the canonical distribution, $P(E, T_c)$ is shown as the inset. In Fig. 22 b are the internal and free energies. The abrupt change in the internal energy at 301 K shows that the phase transition is first-order. This is also shown by the double peak in the plot of the logarithm of the canonical distribution, $\log P(E, T_c)$, versus energy at the critical temperature, T_c , (Fig. 22a, inset), as well as by the singularity in the specific heat, C_V , at the critical temperature (see Fig. 23). [It is noted that the results in Fig. 23 were obtained using a

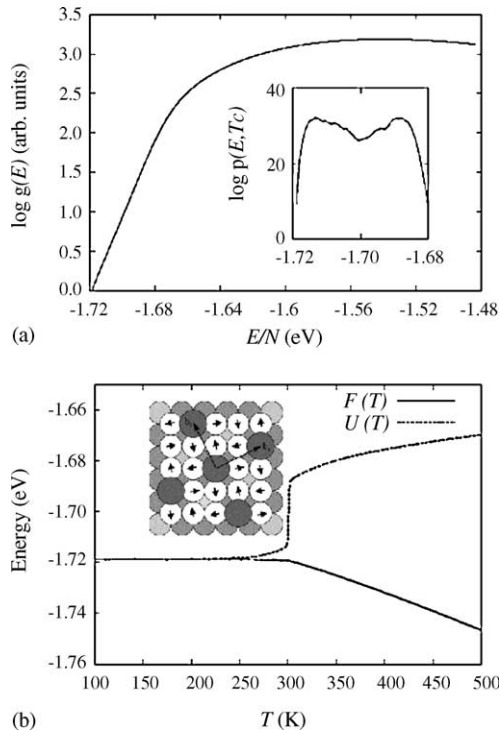


Fig. 22. (a) Density of configurational states (CDOS) as a function of energy for $\theta_{\text{Na}} = 0.2$ ML. Inset: the logarithm of the canonical distribution $P(E, T) = g(-E)e^{E/k_B T}$, at the critical temperature. (b) Free energy $F(T)$ and internal energy $U(T)$ as a function of temperature, derived from DOS. The cusp in $F(T)$ and discontinuity in $U(T)$ at 301 K indicate the occurrence of the first-order disorder-order phase transition, experimentally observed in the temperature range 220–300 K. Inset: the structure of the $(\sqrt{5} \times \sqrt{5})R27^\circ\text{-Na/Al}(1\ 0\ 0)$ phase at 0.2 ML (from Ref. [106]).

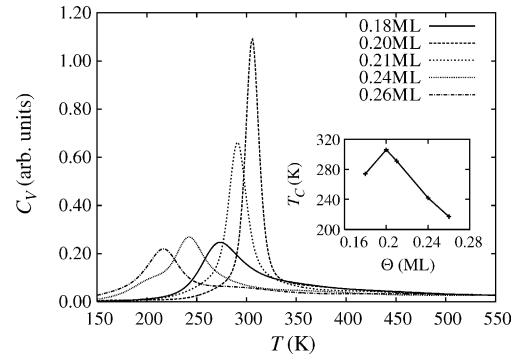


Fig. 23. Specific heat, $C_V(T)$, as obtained from Wang–Landau MC simulations, at different coverages. Inset: critical temperature T_c (as determined from the peak positions) as a function of Na coverage. The highest critical temperature occurs for the $(\sqrt{5} \times \sqrt{5})R27^\circ\text{-Na/Al}(1\ 0\ 0)$ phase at 0.2 ML (from Ref. [106]).

smaller lattice of 20×20 , as compared to 80×80 so that the peaks appear broader. Calculations using the 80×80 for the $\sqrt{5}$ structure at 0.2 ML, yield on the other hand a very sharp peak.] C_V is obtained as”

$$C_V(T) = \frac{(\langle E^2 \rangle_T - \langle E \rangle_T^2)}{T^2}. \quad (12)$$

It can be observed that the experimental phase transition occurs over a rather wide temperature range of around 220–300 K. This could be due to kinetic hindering for atomic processes, e.g. the diffusion of substitutional Na atoms, so that it may be difficult to achieve full thermodynamic equilibrium on the applied measuring times. Also steps could play a role, which are not taken into account in the simulations. Determination of the Na coverage will also be subject to some small uncertainties. In relation to this, it can be seen that the singularity in the specific heat and thus the predicted critical temperature for the order–disorder phase transition, is a sensitive function of the Na coverage, and is a maximum for $\theta_{\text{Na}} = 0.2$ ML corresponding to a surface fully covered with the $(\sqrt{5} \times \sqrt{5})R27^\circ$ phase, reflecting its greater stability. Thus, any experimental deviation to the exact coverage of 0.2 ML, would give rise to a lower observed critical temperature. Fig. 22b shows that the free energy decreases notably with increasing temperature due to the entropic contribution (difference in the free and internal energies). Taking the configurational entropy into account is therefore (and obviously) the crucial aspect in the simulation and understanding of this order–disorder phase transition, and only the LGH + MC approach with its proper sampling of configuration space can provide it.

The LGH + MC approach (or in conjunction with rate equations) obviously does not provide any information as to the dynamics of ‘how’ phase transitions actually take place on the atomic level, nor on what time scale, or if and what kinetic hindering may be involved. For this, one necessarily needs to go beyond a thermodynamic description, and explicitly follow the kinetics of the system over time. The most appropriate method to tackle these questions is by

using the ab initio kinetic Monte Carlo (kMC) approach. Successful studies employing kMC have recently been performed and are reported in Refs. [109–112], which are referred to for details.

6. Conclusion

Recent theoretical results, and methodological approaches and concepts, concerning phase transformations at surfaces have been discussed. In particular, using “straight” DFT, investigations into the trends of the initial incorporation of oxygen into a series of late 4d TM surfaces, Ru(0 0 0 1), Rh(1 1 1), Pd(1 1 1), and Ag(1 1 1) were described. A close correlation between the coverage at which this occurs, with that above which the bulk oxide becomes thermodynamically stable was identified, thus suggesting that the initial incorporation of oxygen actuates the formation of a surface-oxide. This “critical coverage” was found to be lower for the softer metals towards the right of the series. This trend arises due to an interplay of the particular O–metal bond-strength, deformation energy cost for sub-surface occupation, and the build-up of strong repulsive on-surface interactions between the oxygen atoms with increasing coverage.

Focussing on the “extremes” of the studied TM series, O/Ag(1 1 1) and O/Ru(0 0 0 1) systems, the ab initio atomistic thermodynamics approach was applied to calculate free energy, from which the stability range of surface structures were predicted. The main limitation of this method is that its predictive power is limited to the explicitly considered surface structures. For both of the studied systems, and indeed also for O/Rh(1 1 1) and O/Pd(1 1 1) as reported in the literature, the trend found is as follows: with increasing oxygen concentration, firstly on-surface, chemisorbed oxygen occurs, followed by the formation of thin surface-oxide-like structures, which may or may not be commensurate with the underlying metal substrate, and may or may not represent a thermodynamically stable phase. Finally, thicker, more bulk-like films are predicted. For O/Ag(1 1 1) and O/Pd(1 1 1), the thin surface-oxide-like configurations represent stable phases, while those for O/Rh(1 1 1) and O/Ru(0 0 0 1) are only metastable with respect to bulk oxide formation. That ‘metastable’ surface-oxides can in fact form under certain (p, T) conditions, due to kinetic hindering effects, has been demonstrated by combined experimental and theoretical studies for the O/Rh(1 1 1) system. In many (if not all) cases surface-oxide formation induces significant geometrical changes, resulting in structures that have little resemblance to the corresponding bulk oxide. This indicates that they may possess new and interesting properties of importance for technological applications.

Using the concept of a Lattice-gas Hamiltonian (LGH) in combination with either analytical rate equations, or equilibrium Monte Carlo (MC) simulations, represents a so-called “multi-scale” approach, in which meso- or macroscopic properties can be determined on the basis of ab initio

microscopic electronic structure calculations. It affords a greater predictive ability than ab initio atomistic thermodynamics, in that unanticipated structures can be found; also, coexistence and order–disorder phase transitions can be described, and configurational entropy is included. This approach was demonstrated for the O/Ru(0 0 0 1) system where temperature-programmed desorption spectra were obtained, as well as the surface phase-diagram.

Application of the LGH + MC methodology was also discussed for Na on Al(0 0 1), where in particular, an order–disorder temperature-induced phase transition was investigated using the recently introduced MC scheme of Wang and Landau. This algorithm enables direct evaluation of the density of (configurational) states, and thus straightforward determination of the main thermodynamic functions. This approach successfully reproduced the stoichiometry and the temperature at which the transition occurs, and demonstrated the crucial role, and magnitude of, the configurational entropy.

Over the last few years there has been a considerable increase in the atomic level understanding of the behavior of surfaces under “realistic” conditions, which has arisen primarily due to the synergy between experiment and first-principles-based studies. It is envisaged that this trend will continue, with the theoretical methods described here proving very valuable, and this hitherto relatively little studied area will yield many exciting discoveries in the future.

Acknowledgments

Fruitful collaboration with Wei-Xue Li, Micke Borg, Juergen Kreuzer, Stephen Payne, Jean-Sabin McEwen, Karsten Reuter, Veronica Ganduglia-Pirovano, Mira Todorova, and particularly Matthias Scheffler, in addition for continued support, is gratefully acknowledged.

References

- [1] C. Stampfl, M.V. Ganduglia-Pirovano, K. Reuter, M. Scheffler, *Surf. Sci.* 500 (2002) 368.
- [2] K. Reuter, C. Stampfl, M. Scheffler, *Ab initio atomistic thermodynamics and statistical mechanics of surface properties and functions*, in: S. Yip, (Ed.), *Handbook of Materials Modeling, Fundamental Models, Methods*, Vol. 1, Kluwer, in press.
- [3] N. Metropolis, A.W. Rosenbluth, M.N. Rosenbluth, A.H. Teller, E. Teller, *J. Chem. Phys.* 21 (1953) 1087.
- [4] D.P. Landau, K. Binder, *A guide to Monte Carlo simulations in statistical physics*, Cambridge University Press, Cambridge, 2002.
- [5] F. Wang, D.P. Landau, *Phys. Rev. Lett.* 86 (2001) 2050; F. Wang, D.P. Landau, *Phys. Rev. E* 64 (2001) 056101; B.J. Schulz, K. Binder, M. Müller, D.P. Landau, *Phys. Rev. E* 67 (2003) 067102.
- [6] R.M. Dreizler, E.K.U. Gross, *Density-Functional Theory*, Springer, Berlin, 1990.
- [7] R.G. Parr, W. Yang, *Density-Functional Theory of Atoms and Molecules*, Oxford University Press, Oxford, 1994.
- [8] P. Hohenberg, W. Kohn, *Phys. Rev. B* 136 (1964) 864.

- [9] W. Kohn, L. Sham, *Phys. Rev. A* 140 (1965) 1133.
- [10] J.P. Perdew, K. Burke, M. Ernzerhof, *Phys. Rev. Lett.* 77 (1996) 3865.
- [11] J.P. Perdew, J.A. Chevary, S.W. Vosko, K.A. Jackson, M.R. Pederson, D.J. Singh, C. Fiolhais, *Phys. Rev. B* 46 (1992) 6671.
- [12] P. Blaha, K. Schwarz, J. Luitz, WIEN97 (Technical Universität Wien, Austria, 1999), ISBN 3-9501031-0-4.
- [13] M. Bockstedte, A. Kley, J. Neugebauer, M. Scheffler, *Comput. Phys. Commun.* 107 (1997) 187.
- [14] G. Ertl, H. Knözinger, J. Weitkamp (Eds.), *Handbook of Heterogeneous Catalysis*, Wiley, New York, 1997.
- [15] G. Ertl, *J. Mol. Catal. A* 182 (2002) 5.
- [16] T. Engel, G. Ertl, Oxidation of carbon monoxide, in: D.A. King, D.P. Woodruff (Eds.), *The Chemical Physics of Solid Surfaces and Heterogeneous Catalysis*, Elsevier, Amsterdam, 1982.
- [17] V.E. Henrich, P.A. Cox, *The Surface Science of Metal Oxides*, Cambridge University Press, Cambridge, 1993.
- [18] A.T. Fromhold, *Theory of Metal Oxidation*, Vols. I & II, North-Holland, Amsterdam, 1976.
- [19] F. Besenbacher, J.K. Nørskov, *Prog. Surf. Sci.* 44 (1993) 5.
- [20] D.P. Woodruff, T.A. Delchar, *Modern Techniques of Surface Science*, 2nd ed., Cambridge University Press, Cambridge, 1994.
- [21] H. Over, Y.D. Kim, A.P. Seitsonen, S. Wendt, E. Lundgren, M. Schmid, P. Varga, A. Morgante, G. Ertl, *Science* 287 (2000) 1474.
- [22] B.L.M. Hendriksen, S.C. Bobaru, J.W.M. Frenken, *Surf. Sci.* 552 (2004) 229;
B. L.M. Hendriksen, *Model catalysts in action: high-pressure scanning tunneling microscopy*, Ph.D. thesis, Universiteit Leiden (2003).
- [23] B.L.M. Hendriksen, J.W.M. Frenken, *Phys. Rev. Lett.* 89 (2002) 046101.
- [24] H. Over, M. Muhler, *Prog. Surf. Sci.* 72 (2003) 3.
- [25] W.-X. Li, C. Stampfl, M. Scheffler, *Phys. Rev. Lett.* 90 (2003) 256102.
- [26] W.-X. Li, C. Stampfl, M. Scheffler, *Phys. Rev. B* 68 (2003) 165412.
- [27] C.I. Carlisle, T. Fujimoto, W.S. Sim, D.A. King, *Surf. Sci.* 470 (2000) 15.
- [28] C.I. Carlisle, D.A. King, M.L. Boucquet, J. Cerdá, P. Sautet, *Phys. Rev. Lett.* 84 (2000) 3899.
- [29] E. Lundgren, G. Kresse, C. Klein, M. Borg, J.N. Andersen, M. De Santis, Y. Gauthier, C. Konvicka, M. Schmid, P. Varga, *Phys. Rev. Lett.* 88 (2002) 246103.
- [30] E. Lundgren, J. Gustafson, A. Mikkelsen, J.N. Andersen, A. Stierle, H. Dosch, M. Todorova, J. Rogal, K. Reuter, M. Scheffler, *Phys. Rev. Lett.* 92 (2004) 046101.
- [31] M. Todorova, E. Lundgren, V. Blum, A. Mikkelsen, S. Gray, J. Gustafson, M. Borg, J. Rogal, K. Reuter, J.N. Andersen, M. Scheffler, *Surf. Sci.* 541 (2003) 101.
- [32] J. Gustafson, A. Mikkelsen, M. Borg, E. Lundgren, L. Köhler, G. Kresse, M. Schmid, P. Varga, J. Yuhara, X. Torrelles, C. Quiros, J.N. Andersen, *Phys. Rev. Lett.* 92 (2004) 126102.
- [33] W.-X. Li, L. Österlund, E.K. Vestergaard, R.T. Vang, J. Matthiesen, T.M. Pedersen, E. Lgsgaard, B. Hammer, F. Besenbacher, *Phys. Rev. Lett.* 93 (2004) 146104.
- [34] S. Surnev, G. Kresse, M.G. Ramsey, F.P. Netzer, *Phys. Rev. Lett.* 87 (2001) 086102.
- [35] O. Dulub, W. Hebenstreit, U. Diebold, *Phys. Rev. Lett.* 84 (2000) 3646.
- [36] S.A. Chambers, *Surf. Sci. Rep.* 39 (2000) 105.
- [37] R. Franci, *Surf. Sci. Rep.* 38 (2000) 195.
- [38] G.C. Bond, S.F. Tahir, *Appl. Catal.* 71 (1991) 1.
- [39] G. Centi, *Appl. Catal. A* 147 (1996) 267.
- [40] M. Todorova, W.-X. Li, M.V. Ganduglia-Pirovano, C. Stampfl, K. Reuter, M. Scheffler, *Phys. Rev. Lett.* 89 (2002) 096103.
- [41] M. Scheffler, C. Stampfl, *Theory of adsorption on metal substrates*, in: K. Horn, M. Scheffler (Eds.), *Handbook of Surface Science*, Vol. 2. Electronic Structure, Elsevier, Amsterdam, 2000.
- [42] Y. Zhang, W. Yang, *Phys. Rev. Lett.* 80 (1998) 890.
- [43] J.P. Perdew, S. Kurth, A. Zupan, P. Blaha, *Phys. Rev. Lett.* 82 (1999) 2544.
- [44] C. Stampfl, H.J. Kreuzer, S.H. Payne, M. Scheffler, *Appl. Phys. A* 69 (1999) 471.
- [45] W.-X. Li, C. Stampfl, M. Scheffler, *Phys. Rev. B* 65 (2002) 075407.
- [46] P.W. Anderson, *Phys. Rev.* 124 (1961) 41.
- [47] T.B. Grimley, *J. Vac. Sci. Technol.* 8 (1971) 21.
- [48] D.M. News, *Phys. Rev.* 178 (1969) 1123.
- [49] J.K. Nørskov, *Rep. Prog. Phys.* 53 (1990) 1253.
- [50] B. Hammer, J.K. Nørskov, *Adv. Catal.* 45 (2001) 71.
- [51] Experimental heats of formation (eV/O atom): $\Delta H_f = 1.59$ eV (RuO₂), 1.19 eV (Rh₂O₃), 0.88 eV (PdO), and 0.34 eV (Ag₂O) in: *CRC Handbook of Chemistry and Physics*, 76th ed., CRC Press, Boca Raton, FL, 1995.
- [52] K. Reuter, M.V. Ganduglia-Pirovano, C. Stampfl, M. Scheffler, *Phys. Rev. B* 65 (2002) 165403.
- [53] W.-X. Li, C. Stampfl, M. Scheffler, *Phys. Rev. B* 67 (2003) 045408.
- [54] M.V. Ganduglia-Pirovano, K. Reuter, M. Scheffler, *Phys. Rev. B* 65 (2002) 245426.
- [55] M. Todorova, K. Reuter, M. Scheffler, *Phys. Rev. B*, in press.
- [56] K.D. Gibson, M. Viste, E.C. Sanchez, S.J. Sibener, *J. Chem. Phys.* 110 (1999) 2757.
- [57] A. Böttcher, H. Niehus, S. Schwegmann, H. Over, G. Ertl, *J. Phys. Chem. B* 101 (1997) 11185.
- [58] C. Stampfl, S. Schwegmann, H. Over, M. Scheffler, G. Ertl, *Phys. Rev. Lett.* 77 (1996) 3371.
- [59] J. Wider, T. Greber, E. Wetli, T.J. Kreuzer, P. Schwaller, J. Osterwalder, *Surf. Sci.* 417 (1998) 301.
- [60] P. Sabatier, *Berichte der Deutschen Chem. Gesellschaft* 44 (1911) 1984.
- [61] H. Toulhoat, P. Raybaud, S. Kasztelan, G. Kresse, J. Hafner, *Catal. Today* 50 (1999) 629.
- [62] A. Nagy, G. Mestl, D. Herein, G. Weinberg, E. Kitzelmann, R. Schlögl, *J. Catal.* 182 (1999) 417;
A. Nagy, G. Mestl, D. Herein, G. Weinberg, E. Kitzelmann, R. Schlögl, *J. Catal.* 188 (1999) 58;
A. Nagy, G. Mestl, D. Herein, G. Weinberg, E. Kitzelmann, R. Schlögl, *Appl. Catal. A* 188 (1999) 337.
- [63] D. Herein, A. Nagy, H. Schubert, G. Weinberg, E. Kitzelmann, R. Schlögl, *Z. Phys. Chem.* 197 (1996) 67.
- [64] R.A. van Santen, H.P.E.E. Kuipers, *Adv. Catal.* 35 (1987) 265.
- [65] A.I. Boronin, V.I. Avdeev, S.V. Koshcheev, K.T. Murzakhmetov, S.F. Ruzankin, G.M. Zhidomirov, *Kinet. Katal.* 40 (1999) 721.
- [66] X. Bao, M. Muhler, Th. Schedel-Niedrig, R. Schlögl, *Phys. Rev. B* 54 (1996) 2249.
- [67] M. Scheffler, J. Koukal, *Physics of Solid Surfaces - 1987*, Elsevier, Amsterdam, 1987.
- [68] M. Scheffler, J. Dabrowski, *Philos. Mag. A* 58 (1988) 107.
- [69] G.-X. Qian, R. Martin, D.J. Chadi, *Phys. Rev. B* 38 (1998) 7649.
- [70] X.-G. Wang, W. Weiss, Sh.K. Shaikhutdinov, M. Ritter, M. Petersen, F. Wagner, R. Schlögl, M. Scheffler, *Phys. Rev. Lett.* 81 (1998) 1038.
- [71] K. Reuter, M. Scheffler, *Phys. Rev. B* 65 (2002) 035406.
- [72] Z. Łodzianan, J.K. Nørskov, *J. Chem. Phys.* 118 (2003) 11179.
- [73] D.R. Stull, H. Prophet, *JANAF Thermochemical Tables*, 2nd ed., U.S. National Bureau of Standards, Washington, DC, 1971.
- [74] A. Michaelides, M.-L. Bocquet, P. Sautet, A. Alavi, D.A. King, *Chem. Phys. Lett.* 367 (2003) 344.
- [75] A. Michaelides, private communication.
- [76] N.W. Cant, P.C. Hicks, B.S. Lennon, *J. Catal.* 54 (1978) 372.
- [77] C.H.F. Peden, D.W. Goodman, *J. Phys. Chem.* 90 (1986) 1360.
- [78] T.E. Madey, H.A. Engelhardt, D. Menzel, *Surf. Sci.* 48 (1975) 304.
- [79] C. Stampfl, H.J. Kreuzer, S.H. Payne, H. Pfnür, M. Scheffler, *Phys. Rev. Lett.* 83 (1999) 2993.
- [80] L. Surnev, G. Rangelov, G. Bliznakov, *Surf. Sci.* 159 (1985) 299.

- [81] C. Stampfl, M. Scheffler, *Phys. Rev. B* 54 (1996) 2868.
- [82] K. Reuter, C. Stampfl, M.V. Ganduglia-Pirovano, M. Scheffler, *Chem. Phys. Lett.* 352 (2002) 311.
- [83] A. Böttcher, H. Conrad, H. Niehus, *Surf. Sci.* 425 (2000) 125.
- [84] K. Reuter, M. Scheffler, *Phys. Rev. Lett.* 90 (2003) 046103.
- [85] Y.D. Kim, H. Over, G. Krabbes, G. Ertl, *Top. Catal.* 14 (2001) 95.
- [86] R. Blume, H. Niehus, H. Conrad, A. Böttcher, *J. Chem. Phys.* 120 (2004) 3871.
- [87] M. Todorova, Oxidation of Palladium Surfaces, Ph.D. thesis, Technical University Berlin, 2004.
- [88] D. De Fontaine, P.E.A. Turchi, A. Gonis, *Statics and Dynamics of Alloy Phase Transformations*, NATO ASI Series, Plenum Press, New York, 1994.
- [89] J.M. Sanchez, F. Ducastelle, D. Gratias, *Physica A* 128 (1984) 334.
- [90] A. Zunger, P.E.A. Turchi, A. Gonis, *Statics and Dynamics of Alloy Phase Transformations*, NATO ASI Series, Plenum Press, New York, 1994.
- [91] A. van de Walle, G. Ceder, *J. Phase Equilib.* 23 (2002) 348.
- [92] P. Piercy, K. De'Bell, H. Pfnür, *Phys. Rev. B* 45 (1992) 1869.
- [93] G.M. Xiong, C. Schwennicke, H. Pfnür, H.-U. Everts, *Z. Phys. B* 104 (1997) 529.
- [94] V.P. Zhdanov, B. Kasemo, *Surf. Sci.* 415 (1998) 403.
- [95] S.-J. Koh, G. Ehrlich, *Phys. Rev. B* 60 (1999) 5981.
- [96] L. Österlund, M. Pedersen, I. Stensgaard, E. Lægsgaard, F. Besenbacher, *Phys. Rev. Lett.* 83 (1999) 4812.
- [97] S.H. Payne, H.J. Kreuzer, W. Frie, L. Hammer, K. Heinz, *Surf. Sci.* 421 (1999) 279.
- [98] H.J. Kreuzer, S.H. Payne, M. Borowko, *Computational Methods in Surface and Colloid*, Marcel Dekker, New York, 2000.
- [99] H.J. Kreuzer, S.H. Payne, W. Rudziński, W.A. Steele, G. Zgrablich, *Equilibria and Dynamics of Gas Adsorption on Heterogeneous Solid Surfaces*, Vol. 104, Elsevier, 1997.
- [100] M. Gsell, M. Stichler, P. Jakob, D. Menzel, *Isr. J. Chem.* 38 (1999) 339.
- [101] Y.D. Kim, S. Wendt, S. Schwegmann, H. Over, G. Ertl, *Surf. Sci.* L138 (1997).
- [102] J.-S. McEwen, S.H. Payne, C. Stampfl, *Chem. Phys. Lett.* 361 (2002) 317.
- [103] D.L. Adams, *Appl. Phys. A* 62 (1996) 123.
- [104] R.D. Diehl, R. Mc Grath, *J. Phys. Condens. Mat.* 9 (1997) 951.
- [105] C. Stampfl, M. Scheffler, *Surf. Rev. Lett.* 2 (1995) 317.
- [106] M. Borg, C. Stampfl, A. Mikkelsen, J. Gustafson, E. Lundgren, M. Scheffler, J. N. Andersen, *Chem. Phys. Chem.* in press.
- [107] J. Shao, *J. Am. Stat. Assoc.* 88 (1993) 486.
- [108] P. Zhang, *Ann. Stat.* 21 (1993) 299.
- [109] P. Ruggerone, C. Ratsch, M. Scheffler, Density-functional theory of epitaxial growth of metals, in: D.A. King, D.P. Woodruff (Eds.), *Growth and Properties of Ultrathin Epitaxial Layers. The Chemical Physics of Solid Surfaces*, vol. 8, Elsevier, Amsterdam, 1997.
- [110] P. Kratzer, M. Scheffler, *Phys. Rev. Lett.* 88 (2002) 036102.
- [111] K. Reuter, D. Frenkel, M. Scheffler, *Phys. Rev. Lett.* 93 (2004) 116105.
- [112] P. Kamakoti, B.D. Morreale, M.V. Ciocco, B.H. Howard, R.P. Killmeyer, A.V. Cugini, D.S. Sholl, *Science* 307 (2005) 569.